

**U.S. DEPARTMENT OF COMMERCE
National Oceanic and Atmospheric Administration
Environmental Research Laboratories**

NOAA Technical Memorandum ERL NSSL 64

**METEOROLOGICAL RADAR SIGNAL
INTENSITY ESTIMATION**

Dale Sirmans
R. J. Doviak

**Property of
NWC Library**
University of Oklahoma

National Severe Storms Laboratory
Norman, Oklahoma
September 1973



TABLE OF CONTENTS

	<u>Page</u>
LIST OF FIGURES	v
LIST OF TABLES	vii
LIST OF SYMBOLS	viii
ABSTRACT	xiii
1. INTRODUCTION	1
2. PROPERTIES OF METEOROLOGICAL RADAR ECHOES	2
2.1 Echo Waveform	2
2.2 Statistical Properties of Receiver Output Signals	3
2.3 Statistical Dependence of the Samples	7
2.3.1 Statistical dependence related to input power spectrum	8
2.4 Velocity Variance Relationships	10
2.5 Estimated Variance Values for a Weather Radar Example	14
2.5.1 Antenna rotation	14
2.5.2 Fall velocity variance	14
2.5.3 Beam broadening	15
2.5.4 Shear	15
2.5.5 Turbulence	15
2.5.6 Composite variance	16
2.6 Number of Equivalent Independent Samples	16
2.6.1 Independent samples due to spectrum variance	17
2.6.2 Independent samples due to sample volume replenishment	17
2.7 Summary	18
3. AVERAGING TECHNIQUES	20
3.1 Range Averaging	22
3.1.1 Range correlation of echo samples	22
3.1.2 Range correlation of noise samples	23
3.1.3 Variance reduction due to range averaging	24
3.2 Time Averaging	25
3.2.1 Digital lowpass filter theory	26
3.2.2 Equivalent time constant and correlation of output estimates	29
4. VARIANCE AND BIAS DUE TO QUANTIZATION	30
4.1 Analog-to-Digital Conversion	30
4.2 Range Averaging	32
4.3 Time Averaging	32

	<u>Page</u>
5. OUTPUT DATA PROPERTIES	35
5.1 Expected Value of Echo Power Associated with the Digital Mean	35
5.2 Variance of the Estimate	37
5.3 Analog Data	40
5.3.1 Correlation and resolution in azimuth	40
5.3.2 Correlation and resolution in range	42
5.4 Digital Data	43
5.4.1 Correlation and resolution in azimuth	43
5.4.2 Correlation and resolution in range	44
5.4.3 Redundancy of the digital data	45
6. SAMPLE RESULTS	46
7. CONCLUSIONS AND SUMMARY	50
8. ACKNOWLEDGMENTS	52
9. REFERENCES	52
APPENDIX A - COMPARISON OF VARIANCE IN THE POWER ESTIMATE OBTAINED FROM THREE TYPES OF RECEIVERS	55
A.1 Square Law Receiver	56
A.2 Logarithmic Receiver	57
A.3 Linear Receiver	60
APPENDIX B - BIAS IN RANGE AVERAGES DUE TO REFLECTIVITY GRADIENTS	63
APPENDIX C - AUTOCORRELATION OF RANGE SAMPLES	69
APPENDIX D - PROPERTIES OF THE DIGITAL LOWPASS FILTER	73
APPENDIX E - CUMULATIVE DISTRIBUTION FOR THE PROBABILITY DENSITY OF THE LOGARITHM OF ECHO POWER	79

LIST OF FIGURES

<u>Figure</u>	<u>Page</u>
1. Illustration of instantaneous echo power versus time.	2
2. Expected velocity spectrum standard deviation, σ_v , for the WSR-57 and WDS-71 radar systems.	16
3. Number ratio, N_I/N_S , of equivalent independent samples to the total number of samples collected versus the velocity spectrum standard deviation, σ_v .	17
4. Correlation coefficient versus azimuthal sample spacing.	18
5. Digital integrator block diagram.	21
6. Echo sample correlation in range (time), τ , for a rectangular pulse illuminating a uniform reflectivity field.	23
7. Number of independent samples, N_{IR} , versus the number of samples, N_R .	25
8. Ratio of signal variance, σ_s^2 , to the signal plus noise variance, σ_{s+n}^2 , versus the signal to noise power ratio, S/N.	26
9. Digital time integrator flow diagram.	27
10. Variance flow diagram for the digital integrator designed for NSSL's WSR-57 radar.	38
11. Ratio of the output sample standard deviation for correlated input samples, σ_d , to that obtained for statistically independent samples, σ_I .	40
12. Normalized output autocorrelation coefficient after averaging, $R_o^{(h)}$, versus angular displacement.	41
13. Spatial scale amplitude weighting function along the radial.	43
14. Ratio of number of output samples, N_S , to the number of statistically independent output samples, N_I , as related to the autocorrelation $R_o^{(h)}$ of the azimuthal samples.	46

<u>Figure</u>	<u>Page</u>
15. PPI display of nonintegrated logarithmic power.	47
16. PPI displays of integrated logarithmic power.	48
A.1. Density function, $f(\hat{P}_i)$, for estimates of mean input power.	58
B.1. Range dependency of echo power for a step change in reflectivity.	64
B.2. Range averaging bias for a step change in reflectivity versus range interval, R_1 .	65
B.3. Range dependency of echo power for an exponential reflectivity distribution.	65
B.4. Range averaging bias for an exponential range power distribution.	67
E.1. Probability distribution of $\log P_i/\bar{P}_i$.	80

LIST OF TABLES

<u>Table</u>	<u>Page</u>
1. Meteorological echo statistics at receiver input.	5
2. Meteorological echo statistics at receiver output.	6
3. Comparison of expected values and standard deviation of estimates \hat{P}_i of mean input power \bar{P}_i .	7
4. Autocorrelation of noise and signal versus the sampling increment-receiver bandwidth product.	24
5. Variance and truncation bias due to quantization for a conversion range of 64 dB.	31
6. Comparative lengths of digital words in the time integrator loop (WSR-57).	33
7. Mean power estimate standard deviation of analog output of the WSR-57 digital integrator.	39
8. Mean power estimate standard deviation of digital output of the WSR-57 digital integrator.	39
D.1. Equivalent time constant for the WSR-57 processor.	75
E.1. Cumulative distribution of probability density of the logarithm of echo power.	80

LIST OF SYMBOLS

<u>Symbol</u>		<u>Page</u>
A	- amplitude transfer	33
B	- 3 dB bandwidth of receiver	23
c	- velocity of light	2
cT_1	- range "time constant"	21
cw	- continuous wave	2
$D_{-3}(-Z^{\frac{1}{2}})$	- parabolic cylinder function	61
$E[\hat{P}_i]$	- expected value input power estimates	7
F_m	- relative frequency of occurrence of m^{th} class	79
$f(\hat{P}_i)$	- probability density function of input power estimates	56
$f_w(W)$	- probability density of single sample estimate	56
$f(\hat{W}_k)$	- probability density of k sample averages	56
g^{-1}	- receiver transfer function	56
h	- spatial pulse length	2
$h(t)$	- unit impulse response	76
k	- number of independent samples	7
K_p	- perpendicular shear (sec^{-1})	13
K_r	- radial shear (sec^{-1})	13
K_R	- radial wave number	43
K_v	- vertical shear (sec^{-1})	13
K_θ	- azimuthal wave number	44
L	- ratio of sampling interval to the effective response time or in terms of the angular increment; $L = \Delta\theta/\Delta T_e$	45
m	- an integer	8
M	- number of digital classes in the analog-to-digital conversion	36

<u>Symbol</u>		<u>Page</u>
N_b	- number of bits in analog to digital conversion	31
N_e	- equivalent number of independent samples	26
N_I	- number of independent samples	7
N_{IR}	- number of independent range samples	25
N_R	- number of range samples	22
N_s	- number of samples averaged	4
P_i	- echo power input	3
\bar{P}_i	- average input power	4
\hat{P}_i	- input power estimate	7
\hat{P}'_i	- unbiased estimate of \bar{P}_i	59
$\langle P_i \rangle$	- spatially averaged estimate	25
P_m	- most probable estimate of \bar{P}_i	58
PRT	- pulse repetition time	2
R	- range to center of V_s (m)	13
rf	- radio frequency	2
R_i	- receiver input resistance	5
r_o	- average radius of eddies	14
$R_o^{(n)}$	- autocorrelation of the integrator output samples	30
$R_o(\tau)$	- autocorrelation function of filter output	76
R_s	- range scale size	43
R_{sc}	- cutoff range scale size	43
$S(f)$	- power spectrum	9
T_a	- equivalent uniform window integration time	75
T_e	- equivalent time constant of digital integrator	30

<u>Symbol</u>		<u>Page</u>
T_s	- sampling interval	8
$\text{VAR}^{\frac{1}{2}}[\hat{P}'_i]$	- standard deviation of unbiased power estimates	7
V_{in}	- n^{th} sample input to time integrator	27
$V_i(t)$	- receiver input voltage envelope	4
V_o	- mean wind velocity at V_s center (m sec^{-1})	12
V_{on}	- n^{th} sample output from time integrator	27
\bar{V}_R	- output of range averager	28
V_s	- sample volume	3
W	- radar receiver output (voltage or current)	3
\bar{W}	- output mean	8
W_k	- k^{th} receiver output sample	55
\hat{W}_k	- output estimate (k independent sample average)	8
\bar{X}	- digital output mean	36
α	- angular velocity of antenna (radians per second)	12
β	- multiplier constant of digital lowpass filter	26
γ	- azimuthal angle relative to wind direction at V_s center	12
$\delta(t)$	- Dirac delta function	75
ΔP_{dB}	- class width in dB	31
ΔR	- range averaging interval	22
ΔV	- elemental volume	2
$\Delta \theta$	- angular displacement, sampling increment	41
ϵ_R	- range averaging bias	63
ϵ_t	- truncation bias	31
θ_e	- elevation angle	12

<u>Symbol</u>		<u>Page</u>
θ_s	- azimuthal scale size	42
θ_{sc}	- "cutoff" scale parameter	42
θ_1	- one-way half-power beam width (radians)	12
θ_2	- two-way half-power beam width (radians)	12
λ	- radar wavelength	2
$\rho(mT_s)$	- normalized autocorrelation of samples	8
ρ_N	- autocorrelation of noise	24
ρ_s	- autocorrelation of signal	24
σ_a^2	- analog variance	37
σ_b^2	- variance due to beam broadening ($m^2 \text{ sec}^{-2}$)	11
σ_d^2	- variance due to different drop size fall speed ($m^2 \text{ sec}^{-2}$)	12
σ_E^2	- estimate variance	37
σ_f^2	- predetection frequency spectrum variance (Hz^2)	9
σ_I	- output sample standard deviation for independent samples	40
σ_i^2	- variance of input to the averager	25
σ_n^2	- noise variance	25
σ_{oc}^2	- variance of output with $R_o^{(n)}(KL) = 0$ (independent samples)	45
σ_q^2	- quantization variance (dB^2)	31
σ_{q5}^2	- variance due to 6 bit roundoff for recording	37
σ_r^2	- variance due to antenna rotation ($m^2 \text{ sec}^{-2}$)	11
σ_s^2	- variance due to shear ($m^2 \text{ sec}^{-2}$)	11
σ_{sp}^2	- variance due to shear perpendicular to beam axis ($m^2 \text{ sec}^{-2}$)	12

<u>Symbol</u>		<u>Page</u>
σ_{sr}^2	- variance due to radial shear ($m^2 \text{ sec}^{-2}$)	12
σ_{sv}^2	- variance due to vertical shear ($m^2 \text{ sec}^{-2}$)	12
σ_{s+n}^2	- signal plus noise power estimate variance	25
σ_t^2	- variance due to turbulence ($m^2 \text{ sec}^{-2}$)	11
σ_v^2	- velocity spectrum variance ($m^2 \text{ sec}^{-2}$)	9
σ_w^2	- output sample variance (for single sample estimates of \bar{P}_i)	8
$\sigma^2(\hat{W})$	- output estimate variance (for correlated samples)	8
σ_{wk}^2	- output estimate variance (for k independent sample average)	56
σ_T	- correlation time	9
τ	- time interval	23
τ_p	- transmitted pulse width	2
τ_s	- range sampling increment or time lag	22
$\bar{\varphi}(t)$	- instantaneous phase of input signal	4
ω	- angular velocity	41
ω	- rf angular frequency (radian/sec)	4

ABSTRACT

This memo describes digital integrator processing techniques to reduce the variance of precipitation echo power estimates. The statistical properties of precipitation echoes are reviewed and related to measurements of atmospheric and WSR-57 weather radar parameters. A digital integrator, successfully adapted to the WSR-57, can reduce power estimate variance below 1 dB without compromising the resolution of the WSR-57 radar. Although specific design parameters are tied to the WSR-57 parameters, sufficiently general criteria are developed to permit design engineers to relate these results to other radars. We derive the statistical properties of echo power samples averaged both in range and time. Engineering and meteorological factors affecting the type of averaging technique employed (exponential weighted time average and linear range average) and averaging intervals selected are considered in detail.

The expected value and variance associated with digital data processing due to the analog-to-digital conversion and the arithmetic operations are analyzed. The engineering requirements necessary to insure a minimal signal degradation due to these effects are given.

It is shown that, for integrator parameters used, the variance contributed by the time averaging loop (exponential window function) is small compared with that variance due to range averaging truncation, in turn small compared with the input echo power variance. Relations are derived between integrator and radar parameters and minimum scale of resolved precipitation structure. Sample PPI displays of integrated echo returns from severe convective storms are presented.

METEOROLOGICAL RADAR SIGNAL
INTENSITY ESTIMATION*

Dale Sirmans and R. J. Doviak

1. INTRODUCTION

The capability of radar as an indirect meteorological probe has been recognized for some time and arises from the fact that the average power return from precipitation can be related to rainfall rate. The essentially continuous time and spatial rainfall rate data which the radar can provide over a large geographic area can be applied to hydrologic and water management studies as well as basic studies of weather phenomena.

The widespread application of radar for this purpose has not been realized to date because the large inherent variance of the return signal results in an unacceptable uncertainty of the meteorological measurement. As a result most operational weather radars are used for surveillance and qualitative measurements.

This report describes radar signal averaging using a digital processing technique whereby the mean return signal is estimated to the accuracy required for quantitative meteorological application. A digital processor usually requires less calibration and maintenance than an equivalent analog processor. The digital processing theory presented deals with both range and time (azimuthal) integration of echo samples to estimate reflectivity fields probed by a scanning radar beam. The interdependence between variance reduction of reflectivity estimates, time required to achieve this reduction and spatial correlation of reflectivity is analyzed and a WSR-57 weather radar is used as an example to illustrate the trade-offs between these parameters.

*Work on this project was partially supported by the Federal Aviation Administration under contract DOT FA72-WAI-265.

2. PROPERTIES OF METEOROLOGICAL RADAR ECHOES

The statistical properties of radar echoes returned from precipitation determine the signal processing characteristics required to estimate average values (with prescribed standard deviation) of meteorological parameters, such as rainfall rate, reflectivity factor, etc. This section examines three commonly used receivers and determines their performance in reducing variance. We also formulate relations between velocity variance, radar parameters, and the statistical properties of averaged echo power.

2.1 Echo Waveform

Consider an elemental volume, ΔV , of randomly moving meteorological targets being illuminated with continuous waves (cw) radio frequency (rf) power. The echo power averaged over an rf period (e.g., $\approx 10^{-9}$ sec), assumed short compared with the time required for the targets to move a distance equal to quarter of a wavelength, λ , may have instantaneous values as depicted in figure 1. The rate of echo power fluctuation increases as the rate of reshuffling the targets increases. For the case of pulsed rf illumination where spatial

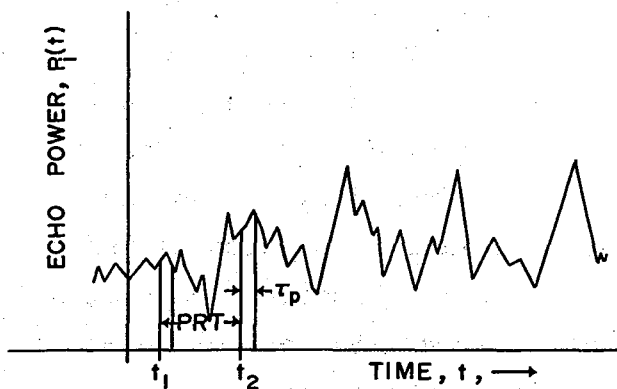


Figure 1. Illustration of instantaneous (averaged over an rf period) echo power versus time for an assumed isolated differential scatter volume illuminated by cw radiation.

pulse width h is large compared with range dimensions of ΔV , the echo power will be samples of the cw signal, figure 1, taken at times t_1 , t_2 , etc., spaced at intervals equal to the pulse repetition time (PRT). The echo power samples will have a time width nearly equal to the transmitted pulse width τ_p . However, as is usual, when meteorological targets occupy a range larger than $h = c\tau_p$, where c is the light velocity, echo power is received continuously for a time

interval twice that spent by the pulse to propagate through the target region. Pulsed rf radiation effectively samples a volume, V_s , of meteorological targets having a range length equal to $c\tau_p/2$ and an angular width nearly equal to the antenna 3 dB beam width (Kerr, 1951; Nathanson, 1969). In section 3 we discuss both: (1) time averages of echo power samples associated with single volumes of range length $c\tau_p/2$ and (2) spatial or range averages of echo power (that is time averages, during a PRT, of power returned from contiguous volumes of range length $c\tau_p/2$). We now consider the statistical properties of the instantaneous power and relate these to the averaging process.

2.2 Statistical Properties of Receiver Output Signals

Precipitation contained within the volume, V_s , sampled by the radar pulse can be considered as a random array of discrete particles each acting as an isotropic scatterer. The power returned from the volume of random scatterers, or targets, is derived by assuming that the relative phase of each target echo is statistically independent of other echoes and distributed uniformly between 0 and 2π . Under this assumption, the average echo power is the sum of the power returned from the individual scatterers. Because echo power fluctuates about this sum, we need to average echo power samples. However, to obtain a large number of independent samples, the average must be made over time periods long compared with that required for particles to be displaced, relative to one another, a distance of $\lambda/4$. The probability densities associated with echo amplitude (i.e., voltage or current) can be shown to be the solution of the two-dimensional Rayleigh "random walk" problem (Marshall and Hitschfeld, 1953).

The output signal amplitude (voltage or current), W , of a radar receiver can have one of many functional dependencies upon the signal amplitude (e.g., voltage) applied to the receiver input port. Common receiver transfer functions are (1) square law, (2) linear, and (3) logarithmic. For example, a square law receiver provides an output, W , that is proportional to the input voltage squared (i.e., echo power input P_i). The probability density of W can be derived from

the density of the input voltage envelope, $V_i(t)$, of the input signal $s(t)$,

$$s(t) = V_i(t) \exp[j(\omega t + \phi(t))] \quad (1)$$

where ω = rf angular frequency (radian/sec), $\phi(t)$ = instantaneous phase (about reference phase ωt) of input signal uniformly distributed over the interval $-\pi, \pi$. Table 1 presents some echo statistics at the receiver input and table 2, the statistics at the output for each of the three receiver transfer functions assuming V_i has a Rayleigh distribution. Also, table 1 shows density functions for the In-phase, I , (real part of $s(t)$) and Quadrature phase, Q , (imaginary part of $s(t)$) components of the input phasor. These density functions have a normal distribution with a variance proportional to the average input power, \bar{P}_i , contributed by V_s . For a pulsed radar \bar{P}_i is defined as

$$\bar{P}_i = \lim_{N_s \rightarrow \infty} \frac{1}{N_s} \sum_{i=1}^{N_s} P_i \quad (2)$$

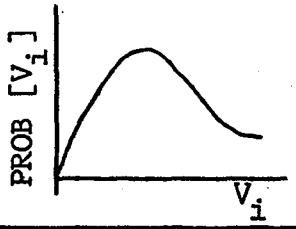
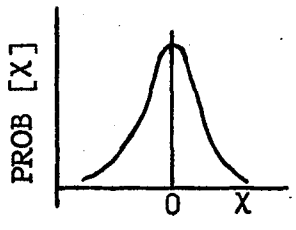
where the N_s samples are obtained at the pulse repetition rate.

For a square law receiver, we note from table 2 that the most probable output amplitude is zero with mean and standard deviation proportional to the average (or mean) input power, \bar{P}_i . On the other hand, the logarithmic receiver has an output voltage (or current) proportional to the log of the input mean power, but a standard deviation independent of input power.

The meteorological parameter required is reflectivity (proportional to \bar{P}_i) from which liquid water content and rainfall rate can be estimated (Battan, 1959). The \bar{P}_i values of meteorological interest may easily span a range of 10^6 and often the choice of receiver type hinges upon this large dynamic range requirement. Because of the relative ease with which a logarithmic transfer function can be realized over the range of \bar{P}_i , logarithmic receivers are usually selected.

However, the need for large dynamic range must be considered in relation to the estimate accuracy for each receiver type. Table 3 shows the expected value and standard deviation (S.D.) of the power

Table 1. Meteorological Echo Statistics at Receiver Input

	PROBABILITY DENSITY	DENSITY PROFILE	MAX. PROB. MODAL VALUE	MEAN VALUE	STANDARD DEVIATION
Input Amplitude $V_i = (X^2 + Y^2)$ $\bar{P}_i = \overline{V_i^2}/R_i^*$	$\frac{2V_i e^{-V_i^2/R_i \bar{P}_i}}{R_i \bar{P}_i}$		$\sqrt{\frac{R_i \bar{P}_i}{2}}$	$\sqrt{\frac{\pi R_i \bar{P}_i}{2}}$	$1/2 \sqrt{(4-\pi) R_i \bar{P}_i}$
Input Quadrature Components (X or Y)	$\frac{e^{-X^2/R_i \bar{P}_i}}{\sqrt{\pi R_i \bar{P}_i}}$		0	0	$\sqrt{\frac{R_i \bar{P}_i}{2}}$

* R_i is the receiver input resistance.

Table 2. Meteorological Echo Statistics at Receiver Output

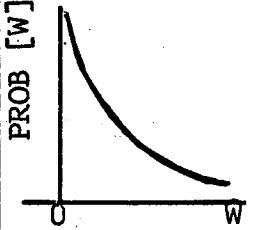
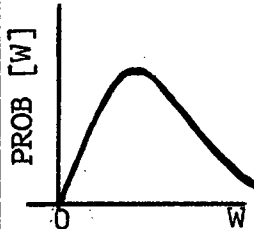
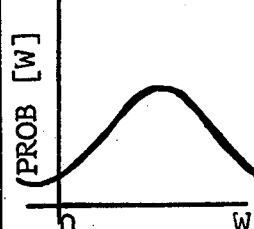
RECEIVER TYPE		PROB [W]	DENSITY PROFILE	MAX. PROB. MODAL VALUE	MEAN VALUE \bar{W}	STD. DEV. σ_W
Square Law	$W = aV_i^2$	$\frac{e^{-W/aR_i\bar{P}_i}}{aR_i\bar{P}_i}$		0	$aR_i\bar{P}_i$	$aR_i\bar{P}_i$
Linear	$W = aV_i$	$\frac{2We^{-W^2/a^2R_i\bar{P}_i}}{a^2R_i\bar{P}_i}$		$.707a R_i\bar{P}_i$	$\frac{a\sqrt{\pi R_i\bar{P}_i}}{2}$	$\frac{a}{2}\sqrt{(4-\pi)R_i\bar{P}_i}$
Logarithmic	$W = b \log(cV_i^2)$ $m = \frac{1}{\log 10}$	$\frac{\exp\left\{\frac{W}{mb} - \frac{e^{W/mb}}{cR_i\bar{P}_i}\right\}}{bmcR_i\bar{P}_i}$		$b \log(cR_i\bar{P}_i)$	$b \log(0.56cR_i\bar{P}_i)$	$.557b$

Table 3. Comparison of Expected Values and Standard Deviation of Estimates \hat{P}_i of Mean Input Power \bar{P}_i .

RECEIVER	DYNAMIC RANGE OF W FOR 10^6 RANGE OF P_i	EXPECTED VALUE OF INPUT POWER ESTIMATES $E[\hat{P}_i]$	S.D. OF INPUT POWER ESTIMATES (UNBIASED) $\text{VAR}^{\frac{1}{2}}[\hat{P}_i']$
Square Law	10^6	\bar{P}_i	P_i/\sqrt{k}
Linear	10^3	$\pi\bar{P}_i/4$	$1.05 \bar{P}_i/\sqrt{k}$
Logarithmic	6	$0.56 \bar{P}_i$	$1.28 \bar{P}_i/\sqrt{k}$

estimates, \hat{P}_i , of \bar{P}_i obtained by averages of k independent samples from each receiver type. The table 3 results are derived in appendix A. Note that only the square law receiver provides an unbiased estimate and has the smallest S.D. Since output averages for both the linear and logarithmic receiver result in a multiplicative bias of the estimates of \bar{P}_i , we must multiply each estimate by the appropriate factor to obtain \bar{P}_i . These estimates have a S.D. (about the unbiased expected value \bar{P}_i) that is tabulated in the table.

Although the logarithmic receiver provides an estimate having the largest S.D. for a given number, k , of independent samples, the number required to achieve a reasonable accuracy is acceptable for most meteorological situations so that antenna scan rate and PRT requirements are not severely compromised. Hereafter we restrict our discussion of digital integrator performance to processing the logarithmic receiver output.

2.3 Statistical Dependence of the Samples

The total number, N_s , of samples obtained from the volume V_s is determined by the antenna beam width, scan rate, and PRT. However, since considerable correlation may exist from sample to sample, we must determine the equivalent number of independent samples, N_I , in

order to estimate the variance reduction indicated in table 3. The degree of correlation between samples is a function of radar parameters, (e.g., wavelength, PRT, beam width, pulse width, etc.) and the meteorological status (e.g., degree of turbulence, shear, etc.) of the sample volume V_s . In the following, we relate these parameters to sample correlation in order to estimate N_I . Although many of the results are well documented in the literature, they are listed here as a convenient reference because they form the basis for the design of the digital integrator.

2.3.1 Statistical dependence related to input power spectrum

If the estimate \hat{W}_k of the output mean \bar{W} is derived from a linear average of k independent samples, the output single sample estimate variance, σ_w^2 (table 2), is reduced by a factor of $1/k$ (appendix A.2). That is

$$\sigma_{wk}^2 \equiv \frac{\sigma_w^2}{k} \quad (3)$$

However if we have N_s samples in which correlation exists from sample to sample, estimate variance $\sigma^2(\hat{W})$ is not reduced in proportion to $1/N_s$. Instead for a stationary process and equi-spaced samples, the estimate variance for the N_s sample average is given by (Nathanson, 1969),

$$\sigma^2(\hat{W}) = \sigma_w^2 \sum_{m=-(N_s-1)}^{N_s-1} \frac{N_s - |m|}{N_s} \rho(\pi m T_s) \quad (4)$$

where $\rho(\pi m T_s)$ is the normalized autocorrelation of the samples, m is an integer, and T_s is the sample interval (PRT). The autocorrelation can be expressed in terms of the power spectrum of the random output, and the parameters of this spectrum (in particular spectral width) can be related to atmospheric and radar system parameters. A Gaussian input spectrum can reasonably approximate spectra associated with precipitation echoes. To rigorously determine the autocorrelation of the output W , we should transform this spectrum by the

receiver transfer function (nonlinear for a logarithmic and square law receiver) to derive the output correlation function needed in (4). However, the system parameters are more readily related to the power spectrum of the input voltage V_i and its corresponding auto-correlation. To simplify the analyses, we restrict the following development to power spectra at the receiver input and assume that the deduced equivalent number of independent samples N_I is equal to that available at a square law receiver output. For this case and a normal distribution of amplitude at the input, the output correlation function is derived (Davenport and Root, 1958) and we assume that log and square law receiver N_I 's are equal.

Assuming the input power spectrum to be Gaussian

$$S(f) = S_0 \exp\left[-\frac{f^2}{2\sigma_f^2}\right]. \quad (5)$$

The normalized autocorrelation function, derived by taking the Inverse Fourier Transform, is

$$R(\tau) = \exp\left[-\frac{\tau^2}{2\sigma_\tau^2}\right]. \quad (6)$$

The parameters σ_τ and σ_f are related by

$$\sigma_\tau = \frac{1}{2\pi\sigma_f} \quad (7)$$

where the quantity σ_f^2 is the pre-detection spectrum variance. The post detection variance, i.e., the variance of the amplitude fluctuation spectra that determines the correlation is $2\sigma_f^2$ (Lhermitte, 1963). The pre-detection frequency spectrum variance is related to velocity variance of the meteorology, σ_v^2 , and to the radar wavelength, λ , by the Doppler equation.

$$\sigma_f^2 = \frac{4\sigma_v^2}{\lambda^2}. \quad (8)$$

Substituting this and accounting for the detection process, we have the correlation

$$\rho(\tau) = \exp\left[-\frac{\tau^2 16\pi^2 \sigma_v^2}{\lambda^2}\right]. \quad (9)$$

Combining (3), (4), and (9), the equivalent number of independent samples, N_I , is expressed as

$$\frac{\sigma^2(\hat{W})}{\sigma_w^2} \equiv (N_I)^{-1} = \sum_{m=-(N_s-1)}^{N_s-1} \frac{N_s - |m|}{N_s^2} \exp\left[-\frac{16\pi^2 \sigma_v^2 (mT_s)^2}{\lambda^2}\right]. \quad (10)$$

For correlated samples the difference between (10) and continuous integration is small (Lhermitte, 1963). Assuming correlated samples and that $N_s T_s \gg 1/\sigma_f$, we can approximate the solution for the number of independent samples by

$$N_I \approx 4\sqrt{\pi} \frac{\sigma_v N_s T_s}{\lambda}. \quad (11)$$

By setting N_I equal to N_s , we find for sampling intervals

$$T_s \geq \frac{\lambda}{4\sqrt{\pi} \sigma_v} \quad (12)$$

all N_s samples are practically independent. Decreasing T_s below this value would cause the samples to become correlated, which would result in N_I decreasing (for fixed N_s) and the averaging process becoming less efficient.

2.4 Velocity Variance Relationships

The velocity variance is a function both of radar system parameters such as beam width, pulse width, wavelength, etc., and the meteorological parameters that describe the distribution of target (e.g., water drops) density and velocity within the sample volume (Sirmans, 1970). Relative radial motion of targets generates variance in the spectrum of input voltage. For example, turbulence produces random relative radial motion of drops within V_s . Wind

shear causes relative radial target motions as will differences in fall speeds of various size drops. There is also a contribution to variance caused by the "apparent" relative motion of targets. As an example, targets moving at uniform speed across the radar sample volume V_s have different radial components of velocity because of the finite size of V_s . This effect, which is more pronounced as V_s gets larger, is known as beam broadening and exists for uniform target motion either perpendicular or parallel to the beam axis; however, the latter is much smaller than the former. In addition, since the sample volume is sweeping through space (due to antenna rotation), the radar does not receive echoes from identical targets on successive samples. This change in target from pulse to pulse results in an apparent fluctuation of radial motion. This is more clearly understood by referring to figure 1 and assuming that we have two contiguous elemental sample volumes ΔV_1 , ΔV_2 , whose return power is statistically independent. The time between independent samples is not only determined by the rate of reshuffling of targets within ΔV_1 (or ΔV_2), but also by the time required for the antenna beam to move from ΔV_1 to ΔV_2 . The power return will change more rapidly, independent of particle motion inside the sample volume, the faster the antenna is rotated. Thus the variance of the spectrum increases in proportion to the antenna angular velocity.

We assume that each of the above variance producing mechanisms are independent of one another, so that the total velocity variance σ_v^2 can be considered as a sum of the variances contributed by each (Lee, 1964). That is,

$$\sigma_v^2 = \sigma_s^2 + \sigma_b^2 + \sigma_r^2 + \sigma_d^2 + \sigma_t^2 \quad (13)$$

where

σ_s^2 = variance due to shear

σ_b^2 = variance due to beam broadening

σ_r^2 = variance due to antenna rotation

σ_d^2 = variance due to different drop size fall speeds
 σ_t^2 = variance due to turbulence.

The components of σ_b^2 , σ_r^2 , and σ_d^2 are related to the radar and meteorological parameters (Nathanson, 1969) as

$$\sigma_b^2 = (0.42V_o\theta_2\sin\gamma)^2 \quad (14)$$

$$\sigma_d^2 = (\sigma_{do}\sin\theta_e)^2 \quad (15)$$

$$\sigma_r^2 = \left(\frac{\alpha\lambda}{10.7\theta_2}\right)^2 \quad (16)$$

where V_o is the mean wind velocity at the center of V_s , γ is the azimuthal angle relative to wind direction at the center, and θ_2 is the two-way half-power beam width in radians for an assumed circularly symmetric antenna pattern having a Gaussian distribution of power. The variance, σ_{do}^2 , is due to the spread in terminal velocity of various size drops falling relative to the air contained in V_s . Lhermitte (1963) has shown that for rain, σ_{do}^2 equals 1.0 (m/sec)^2 and is nearly independent of drop size distribution and rainfall rate. The elevation angle, θ_e , is to beam center, and α is the angular velocity of the antenna in radians per second. It is easily shown that in terms of the usually specified one-way half-power beam width, θ_1 ,

$$\theta_2 = 0.71\theta_1. \quad (17)$$

The wind shear variance term is assumed to be composed of three independent contributions, i.e.,

$$\sigma_s^2 = \sigma_{sv}^2 + \sigma_{sp}^2 + \sigma_{sr}^2, \quad (18)$$

where each term is due to vertical, perpendicular, and radial shear, respectively. The component of variance due to vertical shear is given by (Nathanson, 1969)

$$\sigma_{sv}^2 = (0.42K_v R \theta_2)^2 \quad (19)$$

where K_v is the vertical shear of radial velocity (m/sec/m) and R (in m) is the range to the center of V_s . Equation (19) is only valid for small elevation angles, and for high elevation angles (19) must be replaced by

$$\sigma_{sv}^2 = [0.42K_v R \theta_2 \cos \theta_e]^2 \quad (20)$$

The variance σ_{sp}^2 is produced by gradients in radial velocity measured perpendicular to the vertical plane containing the beam axes. This contribution follows directly from (19) and is

$$\sigma_{sp}^2 = (0.42K_p R \theta_2)^2 \quad (21)$$

where K_p is the perpendicular shear.

Finally, following the development of Sirmans (1970), the variance σ_{sr}^2 is

$$\sigma_{sr}^2 = \frac{K_r^2 h^2}{48} \quad (22)$$

where K_r is the radial gradient of radial velocity (i.e., radial shear) and h is the spatial pulse length ($c\tau$). Combining (17) through (22), we obtain the total variance due to shear,

$$\sigma_s^2 = 0.09\theta_1^2 R^2 (K_p^2 + K_v^2 \cos^2 \theta_e) + \frac{K_r^2 h^2}{48} \quad (23)$$

The variance σ_t^2 due to turbulence is somewhat more difficult to model. Assuming that turbulence is a conglomeration of eddies whose mean diameter is much smaller than the smallest dimension of V_s , and that an average eddy is a solidly rotating, cylindrical mass of air having a mean angular velocity, ω_e , and an axis perpendicular to the beam axis, Sirmans (1970) has shown that the variance is given approximately by

$$\sigma_t^2 = \left(\frac{\omega_e r_o}{2}\right)^2 \quad (24)$$

where r_o is the average radius of the eddies.

2.5 Estimated Variance Values for a Weather Radar Example

In this section estimated values of the variance components are compared to determine if any terms can be neglected in practice. For sake of example, the WSR-57 radar parameters are taken as representative of weather radar systems and used to determine the design criteria for the digital integrator discussed in section 3.

2.5.1 Antenna rotation

The WSR-57 radar operates at a wavelength near 10 cm, and the antenna rotates at an angular rate of 3 rpm. At this angular velocity, the variance due to antenna rotation for the one-way 3 db beam width of 2.2° is determined by substituting into (16).

$$\sigma_r^2 \approx \frac{3(2\pi) \times 10^{-1} \times 57.3}{10.7 \times 60 \times .71 \times 2.2} = 10^{-4} \text{ m}^2 \text{ sec}^{-2}, \quad (25)$$

which can be considered negligible compared with variance estimates that follow.

2.5.2 Fall velocity variance

In meteorological radar measurements of parameters such as rain-fall rate, where elevation angles are typically below 10° , the variance due to the distribution of fall speeds is, upon substitution into (15),

$$\sigma_d^2 < 3.0 (10^{-2}) \text{ m}^2 \text{ sec}^{-2} \quad (26)$$

and can be considered negligible.

2.5.3 Beam broadening

Assuming $\theta = \pi/2$ and a mean wind speed V_0 of 15 m sec^{-1} (e.g., approximately 30 kts) and a half power (one-way) beam width of 2.2° , we obtain from (14),

$$\sigma_b^2 = 3(10^{-2})^2 \text{ m}^2 \text{ sec}^{-2} . \quad (27)$$

2.5.4 Shear

A value of vertical shear K_v , equal to $4 \times 10^{-3} \text{ sec}^{-1}$, has been suggested by Nathanson as appropriate for arbitrarily oriented radars. In severe storms, Crawford and Brown (1972) have found vertical shear values as large as $3 \times 10^{-2} \text{ sec}^{-1}$ and horizontal shears as large as 10^{-2} sec^{-1} . However, for illustration, we assume Nathanson's value as more typical of average vertical shear in precipitation regions. Horizontal shear usually is less than vertical shear, especially in stratiform situations, and for sake of simplifying the estimates, we neglect σ_{sp}^2 as well as σ_{sr}^2 in comparison with σ_{sv}^2 . Thus we obtain by substituting into (23), the estimate of variance due to shear (for θ_e small),

$$\sigma_s^2 \approx (4.6 \times 10^{-5})^2 R^2 \text{ m}^2 \text{ sec}^{-2} \quad (28)$$

where R is the range in meters. By comparing (28) with (25) through (27), except in regions close (i.e., $R < 10 \text{ km}$) to the radar site, we find the contribution to variance from shear predominates.

2.5.5 Turbulence

Variance due to turbulence is difficult to estimate and varies considerably with the type of precipitation being viewed by the radar. Preliminary data obtained at NSSL indicate that σ_t^2 may vary from an

average of $4 \text{ m}^2 \text{ sec}^{-2}$ for a convective system to about $1 \text{ m}^2 \text{ sec}^{-2}$ for stratiform rain. We assume a value of $2 \text{ m}^2 \text{ sec}^{-2}$.

2.5.6 Composite variance

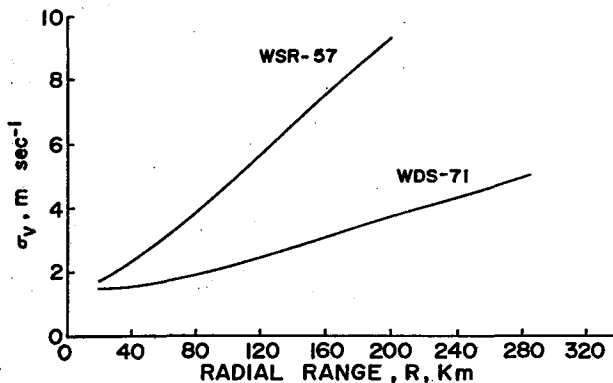
Using the above estimates and neglecting σ_r^2 , σ_d^2 , σ_b^2 , we obtain the following reduced formula for σ_v ,

$$\sigma_v = \sqrt{2 + (4.6 \times 10^{-5})^2 R^2} \text{ m sec}^{-1}, \quad (29)$$

which gives the velocity standard deviation as a function of range R (in m) for the WSR-57 weather radar parameters. Equation (29) is plotted in figure 2. Shown for comparison is the velocity standard deviation computed for NSSL's WDS-71 Doppler radar, which has a one-way beam width of 0.81° and also operates at a wavelength of about 10 cm.

2.6 Number of Equivalent Independent Samples

Results of section 2.3 and 2.4 provide the means for estimating the number of independent samples that may be obtained for given



meteorological and radar parameters. Shorter PRT's (which provide more samples per unit time to estimate mean input power) result in samples having increased correlation, and estimate variance, $\text{VAR}[\hat{P}_i]$, may not be reduced in proportion to the inverse number of samples processed.

Figure 2. Expected velocity spectrum standard deviation, σ_v , for the WSR-57 and WDS-71 radar systems. The radar wavelength is 10 cm and a vertical shear coefficient, K_v , of $4(10^{-3}) \text{ sec}^{-1}$ is assumed.

2.6.1 Independent samples due to spectrum variance

The ratio of the equivalent number, N_I , of independent samples to the number, N_S , of total samples collected versus the standard deviation of the velocity spectrum, σ_V , is shown in figure 3 with the sampling interval, T_S , as a parameter. This is a graph of (10).

2.6.2 Independent samples due to sample volume replenishment

Acquisition of a sample series while the antenna is rotating results in continuous alteration in illumination of the differential scatter volumes contained within the spherical shell of width $c\tau_p/2$. Because the echoes from differential scatter volumes, ΔV , are statistically independent, we can apply the methods outlined in appendix C to show that the echoes from the ΔV 's for two positions of the beam illuminating a uniform reflectivity field are correlated due to a finite two-way beam pattern. Although appendix C derives range sample correlation due to finite pulse width (i.e., range samples may have spacing less than a pulse width), the solution for angular samples is easily executed by exchanging differential range volumes with differential angular volumes and pulse shape with two-way beam pattern. The correlation of angular samples is thus seen to be the correlation between the two-way pattern lagged by the angular sample interval. A good approximation for the antenna pattern is obtained by assuming a uniform illumination of a circular

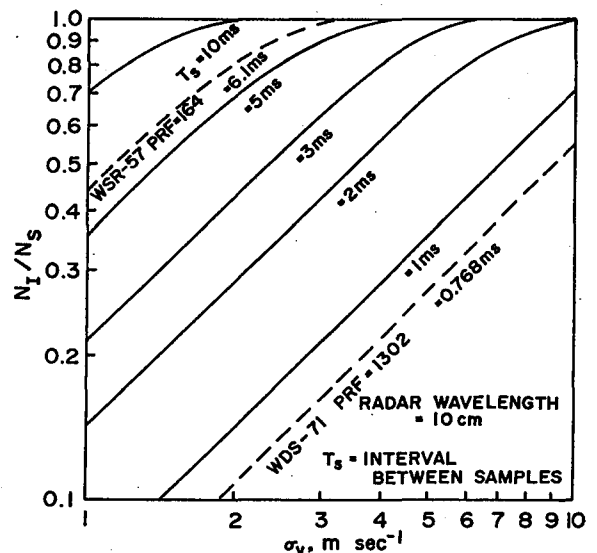


Figure 3. Number ratio, N_I/N_S of equivalent independent samples to the total number of samples collected versus the velocity spectrum standard deviation, σ_V , and the sampling interval, T_S .

aperture (Silver, 1949). Figure 4 shows the autocorrelation coefficient for adjacent samples for this pattern versus the angular sample interval normalized to the one-way half-power beam width. For example, the correlation coefficient between echo samples for the same range but for different beam positions of the WSR-57 operating with an antenna velocity of 3 rpm will be approximately 0.98. At a wavelength of 10 cm and an assumed Gaussian correlation function, this effect would be equivalent for achieving statistical independence to a Doppler variance of approximately $0.18 \text{ m}^2 \text{ sec}^{-2}$.

2.7 Summary

The velocity variance has been related to the radar characteristics and to the meteorological parameters (e.g., shear, turbulence,

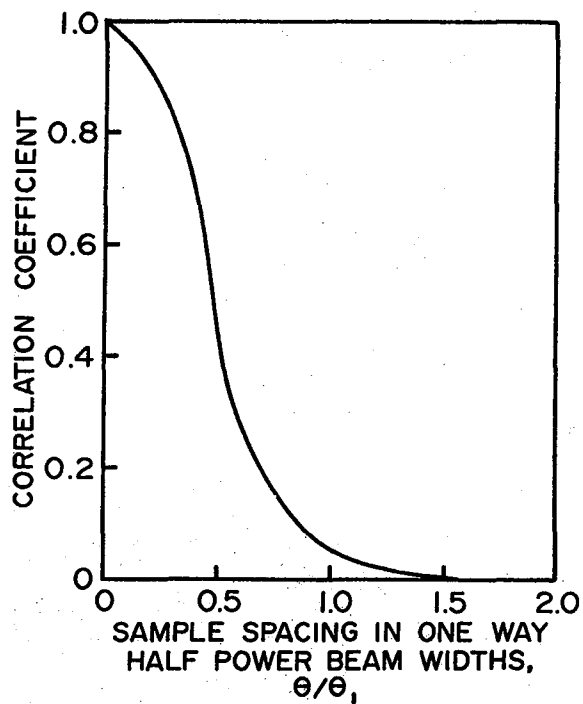


Figure 4. Correlation coefficient versus azimuthal sample spacing in one-way half-power beam width for a uniformly illuminated circular aperture and an uncorrelated, uniform reflectivity field.

etc.) of the sample volume. The radar wavelength and PRT's have been shown to control sample correlation, antenna beam width, and shear control velocity variance, and, along with the transmitter pulse length and dwell time, set bounds on the output data in terms of both resolution and accuracy of reflectivity estimates. If any options are available, these parameters should be adjusted to optimize the processing scheme in terms of the expected velocity variance.

A decrease of wavelength will decrease the time to independence for a given velocity variance, but in general precipitation attenuating the incident power at wavelengths of less than 10 cm makes

quantitative measurements difficult. The PRT, dictated usually by the unambiguous range coverage required for the expected meteorological conditions (i.e., size or range depth of storm) and by average power or duty cycle considerations, is the data sampling rate that determines the correlation of the input samples. From figures 2 and 3, we see that for a 10-cm system with a beam width between 1° and 3°, the PRT, which provides a high rate of practically independent samples, is between 5 msec and 10 msec. Thus the PRT's significantly shorter than this cause the input data to be redundant.

The antenna beam width controls sample correlation by its relation (e.g., (13) and (23)) to velocity variance. A more important property of beam width is the minimum azimuthal and elevation scale resolved by the radar. Therefore, beam width is selected on the basis of the minimum scale of the weather to be resolved and not on sample correlation. Estimates of the lower limits of the precipitation scale, based mainly on high density rainfall gauges, are about 300 to 500 m in the horizontal plane (Nathanson, 1969). Estimates of the lower limit in the vertical are about 3000 to 4000 m. Although it is impractical usually to resolve the horizontal scales at any appreciable range, the beam width should be small compared with the reflectivity scales within the storm.

The desired reduction in variance of mean power estimates quite possibly requires a dwell time in excess of that available by rapid scanning of a large volume of space. There are other means to increase the number of independent samples if dwell time is fixed by beam's angular rotation, and these have been discussed by Marshall and Hitschfeld (1953). One technique that is practical to implement, especially in radar systems containing Klystron amplifiers, is to change frequency from pulse to pulse (frequency agility). Marshall and Hitschfeld predicted and Nathanson verified that a radio frequency change between consecutive pulses by an amount equal to τ_p^{-1} would decorrelate the samples. Wallace (1953) has shown that an increased number of independent samples can be obtained (at the sacrifice in spatial resolution) by averaging over several spatial sample volumes. These

samples can be selected in range or in angular increments, or a combination of both. In the next section we discuss spatial (range) and time averaging techniques.

3. AVERAGING TECHNIQUES

The large inherent variance of precipitation echoes (31 dB^2 at the output of a logarithmic receiver) requires averaging to provide an estimate of the mean signal intensity with the accuracy needed for meteorological interpretation. An estimate of return power having a standard deviation of about 1 dB would be adequate for usual applications. Thus the mean estimate should comprise, in the least, 31 independent samples. Reduction of estimate variance can be achieved through range averaging--an average taken over several sample volumes in range--or time averaging--an average taken over several pulses returned from the same sample volume--or a combination of these two methods. A combination technique is usually more desirable, since it reduces the number of samples provided by either method alone and affords some flexibility in selecting the dimensions of the volume over which averaging is performed (i.e., averaging volume). The averaging volume has range dimension determined by the number of contiguous range samples of length $c\tau_p/2$ used in range averaging and an angular width determined by the antenna beam width, the integration time (i.e., number of PRT intervals spanned in time averaging), and antenna angular velocity. Strictly speaking, range averaging is a time average of return power within one PRT; however, since its time scale corresponds to the range of targets, we define it as a range average.

The choice of sample window function (i.e., rectangular, exponential, etc.) used for weighting the samples depends upon whether range or time averaging is being performed and upon the desired format of the output. An exponentially weighted window is practical to implement and provides a continuous estimate of the mean value (Gold and Rader, 1969). Continuous here implies that the mean output is updated with each new sample, and the output at any time is an average

of previous inputs weighted by the window function. Although a scanning rectangular window provides a continuous output, it requires considerable data storage and thus its cost usually is prohibitive. Averages of time samples in a block can reduce the cost considerably, even though the integration is not strictly continuous (i.e., the rectangular window shifts in time steps equal to time required to collect the sample block) (Hall et al., 1963). This technique is implemented where output averages can be recorded or viewed in discrete steps. The WDS-71 Digital Integrator uses this technique.

Even though the exponential window is advantageous for display and cost, it may not be suitable for range averaging. Reflectivity gradients as large as 20 dB/km are not uncommon, and an exponential range window having a range "time constant" cT_1 may give undesirably large contributions in the interval cT_1 from large reflectivity regions outside cT_1 . These contributions arise from the existence of the exponential tail that weights these large reflectivity regions.

A rectangular window only weights the contribution within the window, and since discreteness in range may not be bothersome for display, a rectangular range window is used in the digital integrator (fig. 5) described in section 3.2. An exponential window is used for time averages.

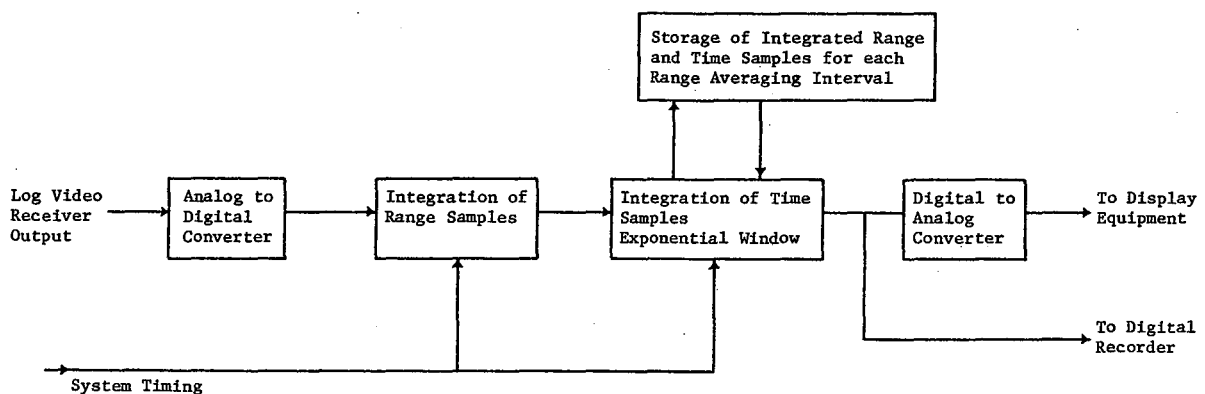


Figure 5. Digital integrator.

The theory of range and time averaging for the digital integrator is given in sections 3.1 and 3.2, respectively. The receiver is assumed to be logarithmic, and its output applied to the digital integrator. Sample correlation and receiver noise influence on integrator performance are analyzed, and relations between integrator, radar, and meteorological parameters are derived. Much of the theory in the following sections applies equally to analog integrators. Digitization and quantization influence on the accuracy of integration is discussed in section 4.

3.1 Range Averaging

The return signal is averaged over a range interval chosen by consideration of the radar's beam width, range at which measurements are to be taken, type of meteorological situations, etc. Range averaging the parameter $\log P_i$ introduces a systematic bias (derived in appendix B) of the estimate caused by reflectivity gradients, which will limit the maximum range interval useful for averaging (Rogers, 1971). Nevertheless, we have a reasonable latitude available in choosing the range interval.

The incremental spacing, τ_s , between samples multiplied by the number of range samples, N_R , averaged gives the range averaging interval, ΔR . The sampling increment is chosen by considerations of the autocorrelation of the consecutive range samples of return signal plus receiver noise. The number of samples in the range interval is restricted to a power of two to facilitate the digital averaging process.

3.1.1 Range correlation of echo samples

The echo sample autocorrelation versus range (fig. 6) is derived in appendix C for an assumed rectangular transmitted pulse, wide band receiver, and uniform reflectivity field. For these conditions, the normalized autocorrelation of echo power is (C.9)

$$\rho_s(\tau) = 1 - \frac{|\tau_s|}{\tau_p} \quad 0 < |\tau_s| < \tau_p$$

$$= 0 \quad \text{otherwise} \quad (30)$$

where τ_s = range sampling increment or lag time. Sampling the echo at time intervals less than the transmitter pulse width results in a successive sample correlation. Nevertheless, usually it is desirable to sample at an increment smaller than the pulse width to reduce the variance contributed by receiver noise. Although this increment results in correlated signal samples and data redundancy, it will not appreciably decrease the overall efficiency or increase integrator cost since the range averaging circuits, being common to all locations, require no pulse-to-pulse storage. If τ_s is small compared with τ_p , we will achieve an estimate variance smaller for the case of noise alone than for signal alone as discussed in the following section.

3.1.2 Range correlation of noise samples

Quite often the bandwidth of the receiver may be about 2 to 3 times the reciprocal of the transmitter pulse width, and since the noise statistics reflect this bandwidth, the noise samples will not be correlated as tightly as the return signal.

If the receiver frequency response is approximated with a Gaussian function, the noise auto-correlation is

$$\rho_N(\tau) = \exp[-7.61(\tau_s B)^2] \quad (31)$$

where B = 3 dB bandwidth of the receiver. Representative values

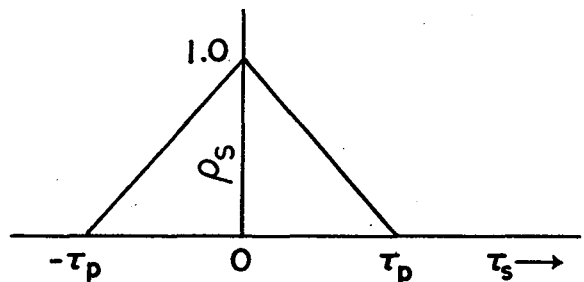


Figure 6. Echo sample correlation in range (time), τ , for a rectangular pulse illuminating a uniform reflectivity field.

of ρ_N and ρ_s are given in table 4 for a receiver bandwidth of two and three times the reciprocal of the transmitter pulse width. The noise samples become significantly correlated for a sampling increment receiver bandwidth product less than about 0.5. Thus sampling increments much less than $0.5/B$ will not result in significant variance reduction. This sampling increment (i.e., $0.5/B$) suggests a range sample increment much smaller than that based solely upon pulse width and signal correlation.

3.1.3 Variance reduction due to range averaging

Averages containing correlated samples (i.e., case of $|\tau_s|/\tau_p < 1$) have an estimate variance, $\sigma^2(\langle P_i \rangle)$, that depends not only on the number, N_R , of samples, but also on sample correlation. The estimate variance in this case is given by (4),

$$\frac{\sigma^2(\langle P_i \rangle)}{\sigma_i^2} = \frac{1}{N_{IR}} = \frac{N_R^{-1}}{\sum_{m=-(N_R-1)}^{N_R-1} \frac{N_R - |m|}{N_R^2} \rho(m\tau_s)}, \quad (32)$$

Table 4. Autocorrelation of Noise and Signal Versus the Sampling Increment-Receiver Bandwidth Product.

$\tau_s B$	Autocorrelation of Noise	Autocorrelation of Signal, ρ_s	
	ρ_N	$\tau_p = 2/B$	$\tau_p = 3/B$
0.1	0.931	0.95	0.967
0.2	0.750	0.90	0.933
0.4	0.317	0.80	0.867
0.5	0.149	0.75	0.834
0.6	0.075	0.70	0.800
0.8	0.010	0.60	0.733
1.0	0.0008	0.50	0.667

where

- $\langle P_i \rangle$ = spatially averaged estimate
- σ_i^2 = variance of input to the averager (i.e., 31 dB²)
- N_{IR} = number of independent range samples
- N_R = number of range samples
- $\rho(m\tau_s)$ = autocorrelation of the samples.

The number of independent range samples, N_{IR} , obtained for various values of τ_s/τ_p is given in figure 7. This number neglects receiver noise and applies without correction (calculated standard error within 10 percent of true standard error) for signal-to-noise ratios, S/N, greater than about 10 dB. For signal levels below this value, the signal plus noise estimate variance, $\sigma_{s+n}^2 (\langle P_i \rangle)$, needs to be corrected as shown in figure 8. This correction comes from weighting the estimate variance, $\sigma_s^2 (\langle P_i \rangle)$, for signal alone and noise variance [i.e., $\sigma_n^2 (\langle P_i \rangle)$] by their respective power weights, dividing each by their respective independent sample number (i.e., N_{IR} and N_R , respectively), and summing the result. The curve in figure 8 assumes $N_{IR}/N_R \ll S/N$ and $S/N \geq 1$. Because noise samples are uncorrelated, the number of independent range samples increases as S/N decreases.

3.2 Time Averaging

The time or pulse-to-pulse averaging of the range averaged signal is accomplished by a digital lowpass filter. The transfer characteristic of this network results in an exponential "time window" and a continuous mean value estimate. A given estimate of course depends on the order of a

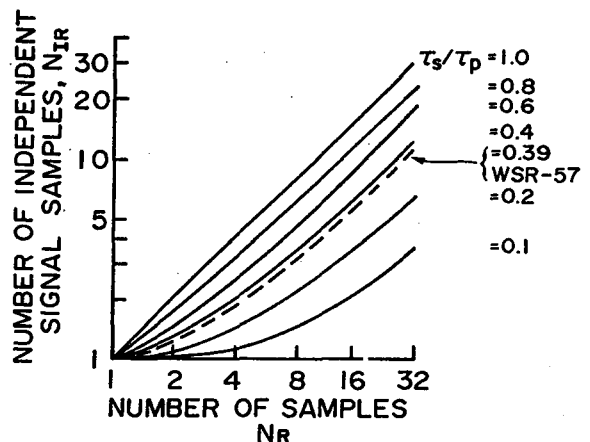


Figure 7. Number of independent samples, N_{IR} , versus the number of samples, N_R , with sampling increment/transmitter pulse width ratio, τ_s/τ_p , as a parameter.

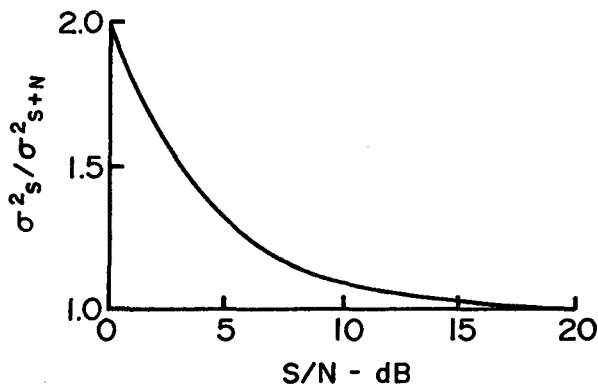


Figure 8. Ratio of signal variance, σ_s^2 , to the signal plus noise variance, σ_{s+n}^2 , versus the signal-to-noise power ratio, S/N.

given input series; but since the order is random, the output estimate is equivalent to a linear averaging over a period determined by the multiplier constant (β) of the digital network. The electronic circuitry required to implement the operation is simplified considerably by limiting the multiplier constant to values given by 2^{-n} where n is an integer.

In this section we discuss the theory of the digital lowpass

filter and compute the statistics of its output.

3.2.1 Digital lowpass filter theory

The following analyses shows that the algorithm describing the digital lowpass filter (appendix D discusses filter properties) provides an unbiased estimate of the input mean (i.e., mean output of range averager). Even though the lowpass filter acts to average an infinite number of possibly independent samples, estimate variance will be finite because sample amplitudes are exponentially weighted. Hence, to obtain estimate variance, we must determine the equivalent number of independent samples, N_e , yielded by the filter. The variance reduction factor (i.e., N_e^{-1}) is derived as a function of β for statistically independent input samples. This is expanded in section 5 to include dependent input samples. To simplify the analyses, we consider the output from one range averaging interval which occurs at periodic intervals equal to a PRT.

The signal flow diagram of the time integrator is depicted in figure 9. The algorithm describing the time integrator is

$$V_{on} = \beta V_{in} + (1 - \beta) V_{o(n-1)} \quad (33)$$

where

- V_{in} = the n^{th} input sample
(output of the range averaging circuit)
- $V_{o(n-1)}$ = the output after
($n-1$) samples
- β = 2^{-n} where $n = 1, 2, 3, \dots$

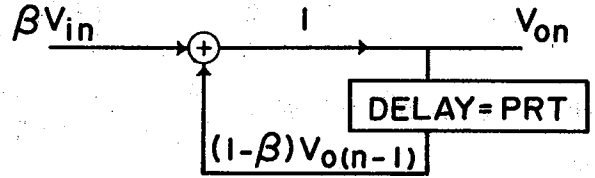


Figure 9. Digital time integrator flow diagram.

Iterating (33) and assuming the boundary value, $V_{o0} = 0$ for $V_{in} = V_{io}$, the output V_{on} may be expressed exclusively in terms of the input as

$$V_{on} = \beta \sum_{m=0}^{n-1} (1 - \beta)^m V_{i(n-m)} \quad (34)$$

When input samples are drawn from a population having a mean value \bar{V}_i , it is clear that

$$\bar{V}_{on} = \beta \bar{V}_i \sum_{m=0}^{n-1} (1 - \beta)^m \quad (35)$$

As (35) approaches steady state (i.e., $n \rightarrow \infty$), the sum becomes an infinite geometric progression with first term value of unity and a common ratio of $(1 - \beta)$. In the limit the output, V_o , is

$$V_o = \lim_{n \rightarrow \infty} \bar{V}_{on} = \bar{V}_i \left[\frac{\beta}{1 - (1 - \beta)} \right] = \bar{V}_i ;$$

thus, the output is the population mean and the algorithm provides an unbiased estimate.

The variance, σ_{on}^2 , of an n sample estimate is expressed as

$$\sigma_{on}^2 = \overline{V_{on}^2} - (\bar{V}_{on})^2 \quad (36)$$

The second moment, $\overline{V_{on}^2}$, is obtained by averaging the square of (35). That is

$$\overline{V_{on}^2} = \beta^2 \sum_{m=0}^{n-1} \sum_{q=0}^{n-1} (1-\beta)^m (1-\beta)^q \overline{V_{i(n-m)} V_{i(n-q)}} \quad (37)$$

The expected value $\overline{V_{i(n-m)} V_{i(n-q)}}$ is given by (Burington and May, 1953)

$$\overline{V_{i(n-m)} V_{i(n-q)}} = \rho_{rs} \sigma_r \sigma_s + \bar{V}_r \bar{V}_s \quad (38)$$

where

$$r = n-m; \quad s = n-q$$

$$\rho_{rs} \sigma_r \sigma_s = \text{covariance of } V_r, V_s$$

$$\rho_{rs} = \text{correlation coefficient}$$

$$\sigma_{r,s} = \text{standard deviation of } V_{ir}, V_{is}$$

$$\bar{V}_{r,s} = \text{first moment about the origin of } V_r, V_s$$

Equation (38) may be simplified by noting that for statistically independent samples (a good assumption for the WSR-57 parameters, see figs. 2 and 3)

$$\rho_{rs} = 1 \quad \text{for } r = s$$

$$\rho_{rs} = 0 \quad \text{for } r \neq s$$

and that $\sigma_r = \sigma_s = \sigma_i$, the standard deviation of the input, and furthermore $\bar{V}_r = \bar{V}_s$ is equal to the mean of the sample population \bar{V}_i . Substitution into (38) results in

$$\overline{V_{i(n-m)} V_{i(n-q)}} = \sigma_i^2 + \bar{V}_i^2 \quad \text{for } r = s \quad (39)$$

$$\overline{V_{i(n-m)} V_{i(n-q)}} = \bar{V}_i^2 \quad \text{for } r \neq s$$

Upon substituting the above into (37), we obtain

$$\overline{V_{on}^2} = \beta^2 (\sigma_i^2 + \bar{V}_i^2) \sum_{p=0}^{n-1} (1-\beta)^{2p} + \bar{V}_i^2 \beta^2 \sum_{m=0}^{n-1} \sum_{\substack{q=0 \\ m \neq q}}^{n-1} (1-\beta)^{m+q} \quad (40)$$

where we have used $r = s = p$. Expanding the first term of (40) into the sum of two series and combining the series containing \bar{V}_i^2 with the second term of (40), the moment expansion reduces to

$$\overline{v_{on}^2} = \beta^2 \sigma_i^2 \sum_{p=0}^{n-1} (1-\beta)^{2p} + \beta^2 \bar{V}_i^2 \sum_{m=0}^{n-1} \sum_{q=0}^{m-1} (1-\beta)^{m+q}. \quad (41)$$

The mean squared value, $(\bar{V}_{on})^2$, is obtained from squaring (35)

$$(\bar{V}_{on})^2 = \beta^2 \bar{V}_i^2 \sum_{m=0}^{n-1} (1-\beta)^m \sum_{p=0}^{n-1} (1-\beta)^p. \quad (42)$$

Substituting (42) and (41) into (36), we obtain

$$\sigma_{on}^2 = \beta^2 \sigma_i^2 \sum_{p=0}^{n-1} (1-\beta)^{2p}. \quad (43)$$

In the steady state (43) can be expressed as a sum of an infinite geometric progression. That is, the output variance σ_o^2 is given by

$$\sigma_o^2 = \lim_{n \rightarrow \infty} \sigma_{on}^2 = \beta^2 \sigma_i^2 \lim_{n \rightarrow \infty} \sum_{p=0}^{n-1} (1-\beta)^{2p} = \frac{\beta^2 \sigma_i^2}{[1-(1-\beta)^2]}. \quad (44)$$

Therefore

$$\frac{\sigma_o^2}{\sigma_i^2} = \frac{\beta}{2-\beta} = \frac{1}{N_e}. \quad (45)$$

Equation (45) relates the input and output variances and defines the equivalent number, N_e , of independent time samples for a given multiplier constant β .

3.2.2 Equivalent time constant and correlation of output estimates

The time integrator response results in an exponential correlation of the successive output averages (i.e., at intervals equal to the PRT) for a given range averaging interval. As shown in appendix D, the

equivalent time constant, T_e , of the digital integrator, approximated by the first two terms of (D.7) is

$$T_e = \frac{2-\beta}{\beta} \frac{T_s}{2} \quad (46)$$

where T_s is the time interval (PRT) between input samples. The normalized autocorrelation of the output is given by (D.16)

$$R_o^{(n)} = \exp \left[-\frac{\tau}{T_e} \right] . \quad (47)$$

Thus samples of the output at time intervals, τ , less than about $3T_e$ result in a redundancy of output data.

4. VARIANCE AND BIAS DUE TO QUANTIZATION

Digital processing introduces a variance and, in some instances, an error (bias) due to uncertainty associated with the digital number. Here we determine the bias magnitude and estimate variance in order to specify the digital word length and processing technique needed to achieve the required estimate accuracy. The digital processing used in the digital integrator can be divided into three steps: (1) analog to digital conversion, (2) range averaging, and (3) time averaging. The expected estimate value (i.e., bias) and variance resulting from these three operations in cascade is derived.

4.1 Analog-to-Digital Conversion

The first operation is the analog-to-digital (A/D) conversion. The conversion should span a received power range of about 60 dB, and assuming a log receiver response and linear quantization, the digital number will represent equal increments of log P. For quantization by truncation, the expected bias associated with this conversion is one-half of a quantization step (Gold and Rader, 1969). Truncation results in a systematic underestimate of true value. If the

quantization is by roundoff, the expected bias is zero. In either case, the variance associated with the conversion (assuming a uniform input probability across the class) is

$$\sigma_q^2 = \frac{(\Delta P_{dB})^2}{12} \quad (48)$$

where σ_q^2 is the variance in dB^2 and ΔP_{dB} is the class width in dB. The variance σ_q^2 of the operation normalized to the input variance, $\sigma_i^2 = 31 \text{ dB}^2$, is shown in table 5 for a conversion range of 64 dBm. Because the quantization variance is statistically independent of signal variance, the two are additive (Lee, 1964). Table 5 shows that conversions, using more than five bits, result in quantization variance that is a negligible fraction of input variance. Smaller class intervals may be needed for improved efficiency in averaging signals with low signal-to-noise ratio (Works and Groginsky, 1970). Truncation bias is a constant fraction of a class width and can be compensated for in system calibration (Austin and Schaffner, 1970).

Table 5. Variance and Truncation Bias due to Quantization for a Conversion Range of 64 dB.

CLASS WIDTH (dB)	NUMBER BITS (N_b)	QUANTIZATION VARIANCE, σ_q^2 (dB^2)	σ_q^2/σ_i^2	TRUNCATION BIAS, ϵ_t (dB)
8	3	5.33	0.172	4
4	4	1.33	0.043	2
2	5	0.35	0.011	1
1	6	0.085	0.003	0.5
1/2	7	0.021	0.001	0.25
1/4	8	0.005	0.0002	0.125

4.2 Range Averaging

The second operation is range averaging, which consists of a linear average of the prescribed number (N_R) of range samples, i.e.,

$$\bar{V}_R = \frac{1}{N_R} \sum_{i=1}^{N_R} V_i . \quad (49)$$

If N_R is restricted to a power of 2, the division in (49) can be performed by a shift in bit weight of $\log_2 N_R$ places to the left of the binary point. In the WSR-57 integrator, \bar{V}_R is truncated to seven bits before time integration. The variance due to this operation (see table 5) is 0.021 dB^2 and the truncation error is 0.25 dB.

4.3 Time Averaging

The third operation, time averaging, requires implementation of the lowpass filter algorithm given by (33). The WSR-57 integrator's algorithm is expanded to three operations expressed as

$$V_{on} = \beta V_{in} + V_{o(n-1)} - \beta V_{o(n-1)} . \quad (50)$$


The multiplier constant β is (for the WSR-57) restricted to the values,

$$\beta = 2^{-n} \quad n = 2, 3, 4, \text{ or } 5 . \quad (51)$$

The multiplications $[\beta V_{in}, \beta V_{o(n-1)}]$ are performed by a shift in bit weight and the subtraction $[V_{o(n-1)} - \beta V_{o(n-1)}]$ is performed in 2's complement.

In a processing loop of this type, the required minimum storage word bit length is given by the sum of the input word bit length and $(-\log_2 \beta)$ bits (Works and Groginsky, 1970). Without truncation or roundoff, the subtractor word length is the same. This is shown in table 6 for the word lengths used in the WSR-57 integrator. The adder word must be truncated to the storage word length (obviously) and this

Table 6. Comparative Lengths of Digital Words in the Time Integrator Loop (WSR-57).

PARAMETER	WORD	PARAMETER SYMBOL
Input Word, 7 bits	IIIIIIII.	V_{in}
Scaled Input, $\beta = 2^{-5}$, 12 bits	00000II.IIIII	βV_{in}
Storage Word, 12 bits	SSSSSSS.SSSSS	$V_{o(n-1)}$
2's Complement of Storage, 17 bits	00000SS.SSSSSSSSSS	$-\beta V_{o(n-1)}$
Subtractor Word, 17 bits	DDDDDDD.DDDDDDDDDD	$V_{o(n-1)} - \beta V_{o(n-1)}$
Adder Word, 17 bits	AAAAAAA.AAAAAAATA	$\beta V_i + (1-\beta)V_{o(n-1)}$
	 Truncation Lines	

may be done either (1) at the output of the subtractor such that the length of the term $(1-\beta)V_{o(n-1)}$ is equal to the storage word length, or (2) at the output of the adder such that the term $\beta V_{in} + (1-\beta)V_{o(n-1)}$ is equal to the storage word, or (3) a combination of both. Since the hardware has a fixed word length, truncation results in an amplitude transfer of the loop that varies with the multiplier constant. For example, if the truncation is made at the output of the subtractor, the amplitude transfer, A , can be expressed as

$$A = \frac{\beta 2^{s+1}}{\beta(2^{s+1} - 1) + 1} \quad (52)$$

where s is the number of storage word bits. If the arithmetic word length is maintained throughout the loop and the result truncated at the output of the adder, the amplitude transfer is given by

$$A = 1 - \frac{1}{2^{s+1}} \quad (53)$$

and is independent of the multiplier constant so long as the minimum storage word criterion is satisfied. The WSR-57 integrator's subtractor word length is maintained for all multiplier constants except 2^{-5} . This results in an amplitude transfer (or bias) of

$$A = 0.9998 \quad \text{for } \beta = 2^{-2}, 2^{-3}, 2^{-4} \quad (54)$$

and

$$A = 0.9961 \quad \text{for } \beta = 2^{-5} . \quad (55)$$

In both cases, this bias is negligible and need not be considered in the calibration procedures (sec. 5.1).

A subtle source of nonnegligible bias is encountered if the minimum storage word criterion is applied to words in the arithmetic loop (fig. 9). To neglect this bias, the subtractor word length must be longer than the storage word. The bias is a function of input word length, β , and also the sample variance at the input to the loop. If sample variance is 31 dB^2 (i.e., no range integration) and the subtractor word is three or more bits longer than the storage word, the bias can be shown to be 0.1 dB, or less for a 2 dB input class width. For example, using the word lengths shown in table 6, this can be shown to be less than 0.03 dB.

The standard deviation associated with the time averaging loop derived from (48) is for a 12 bit ($\Delta P = 1/64 \text{ dB}$ for a 64 dB input power range) truncation,

$$\sigma = 0.0045 \text{ dB} . \quad (56)$$

In conclusion, the variance contributed by the time averaging loop is small compared with that variance due to range averaging truncation, in turn small compared with the input signal variance.

5. OUTPUT DATA PROPERTIES

5.1 Expected Value of Echo Power Associated with the Digital Mean

The mean calculated by the digital integrator is the first moment about the origin of its input samples, i.e., the mean of a series of samples composed of discrete values. These samples are quantized values of a voltage, W , proportional to the logarithm of echo power and have a probability density given in table 2. Also listed in table 2 is the modal value of W , $\text{blog}(cR_i\bar{P}_i)$; its mean $\text{blog}(0.56cR_i\bar{P}_i)$, which is 2.5 dB below the modal value; and its standard deviation of 5.57 dB. The difference between the logarithm of the true mean power, $\log \bar{P}_i$, and the mean of $\log P_i$, $\overline{\log P_i}$, is independent of the mean \bar{P}_i as is the standard deviation of $\log W$.

The difference (bias) between \bar{P}_i and $\log^{-1}[\overline{\log P_i}]$ is one factor that must be considered in the assignment of expected power values to the digital integrator estimates. Another factor that must be considered is the bias introduced from quantization by truncation (sec. 4). A third bias is caused by the finite range of the A/D conversion; as the true mean of the input distribution approaches the conversion range extremes, the difference between calculated and true mean increases. This is due both to power truncation, i.e., saturation at the upper limit, and to the zero weight associated with all inputs below the conversion range lower limit.

Still another factor is receiver transfer characteristic deviation from a logarithmic response, which results in a modification of the probability density, changes the difference between true and calculated mean, and alters the input variance.

For input signals having mean values in a region of the system transfer response, logarithmic from about 6 dB above to about 12 dB below this mean, the expected power value is 2.5 dB plus the truncation bias (table 5) below the true mean. The behavior near conversion

range extremes depends on the system transfer characteristic and the size of the quantization increment.

A calibration procedure, which relates the integrator output-input mean power for the overall system, and the composite influence of all the factors involved, consists of injecting a known input power (having a standard deviation small compared with the quantization interval) to determine the boundary or threshold levels, in units of $10 \log P_i$, of the digital classes. These experimentally determined boundary values are used as the limits for an incremental integration of the theoretical probability density of $\log P_i$. The integral of probability density over the class limits is the relative frequency of occurrence of that class. The sum of the products (relative occurrence frequency times the class weight) is the digital mean. That is;

$$\bar{X} = \sum_{m=0}^M m \int_{t_m}^{t_{m+1}} \text{Prob}\{\log P_i\} d(\log P_i) , \quad (57)$$

where

\bar{X} = digital output mean

M = number of digital classes in the A/D conversion
($M = 2^{N_b} - 1$)

t_m = lower boundary of class m (in dB)

t_0 = $-\infty$

t_{M+1} = $+\infty$

m = class weight (i.e., 0, 1, ... $2^{N_b} - 1$)

N_b = number of bits in the A/D conversions .

Evaluation of (57) requires only a specification of \bar{P}_i to determine the corresponding value of \bar{X} . The entire transfer, i.e., the expected echo power, \bar{P}_i , corresponding to a given \bar{X} , can be determined by "lagging" \bar{P}_i through the conversion range. The integration can be performed by "table lookup" if the class boundaries, B_m , are expressed in units of dB from \bar{P}_i (appendix E).

5.2 Variance of the Estimate

The variance of the integrator output depends on (1) the input variance, (2) the variance due to processing, and (3) the number of independent samples in the average. Range interval and digital multiplier (β) options available to the operator allow an independent choice of the number of range and time samples with a resulting choice of estimate standard error, which we examine in this section.

A variance flow diagram of the WSR-57 integrator (fig. 10) gives the variance associated with each of the operations in the scheme. Since the processing variance is statistically independent, the composite variance is the sum of the individual variances. At any stage, the estimate variance, σ_E^2 , is merely the input signal variance plus the variance due to processing up to that point. The analog output variance, σ_a^2 , can be expressed as

$$\sigma_a^2 = \frac{\sigma_i^2}{N_{IR} N_e} + \frac{\sigma_{q1}^2}{N_R N_e} + \frac{\sigma_{q2}^2}{N_e} + \sigma_{q4}^2 \quad (58)$$

where the above symbols are defined in figure 10 or have been previously defined in the text.

The estimate standard deviation for the analog output is tabulated in table 7 for various operator options of the WSR-57 integrator. The equivalent number, N_e , of independent samples has been computed assuming that samples to the time integrator are statistically independent.

The variance of the digital output can be expressed as

$$\sigma_b^2 = \frac{\sigma_i^2}{N_{IR} N_e} + \frac{\sigma_{q1}^2}{N_R N_e} + \frac{\sigma_{q2}^2}{N_e} + \sigma_{q5}^2 \quad (59)$$

where σ_{q5}^2 is the variance due to the six bit roundoff for recording and is equal to 0.085 dB^2 . Table 8 gives the standard deviation of the digital estimate.

The estimate variance depends on the statistical dependence between, as well as the number of, samples in the estimate. The

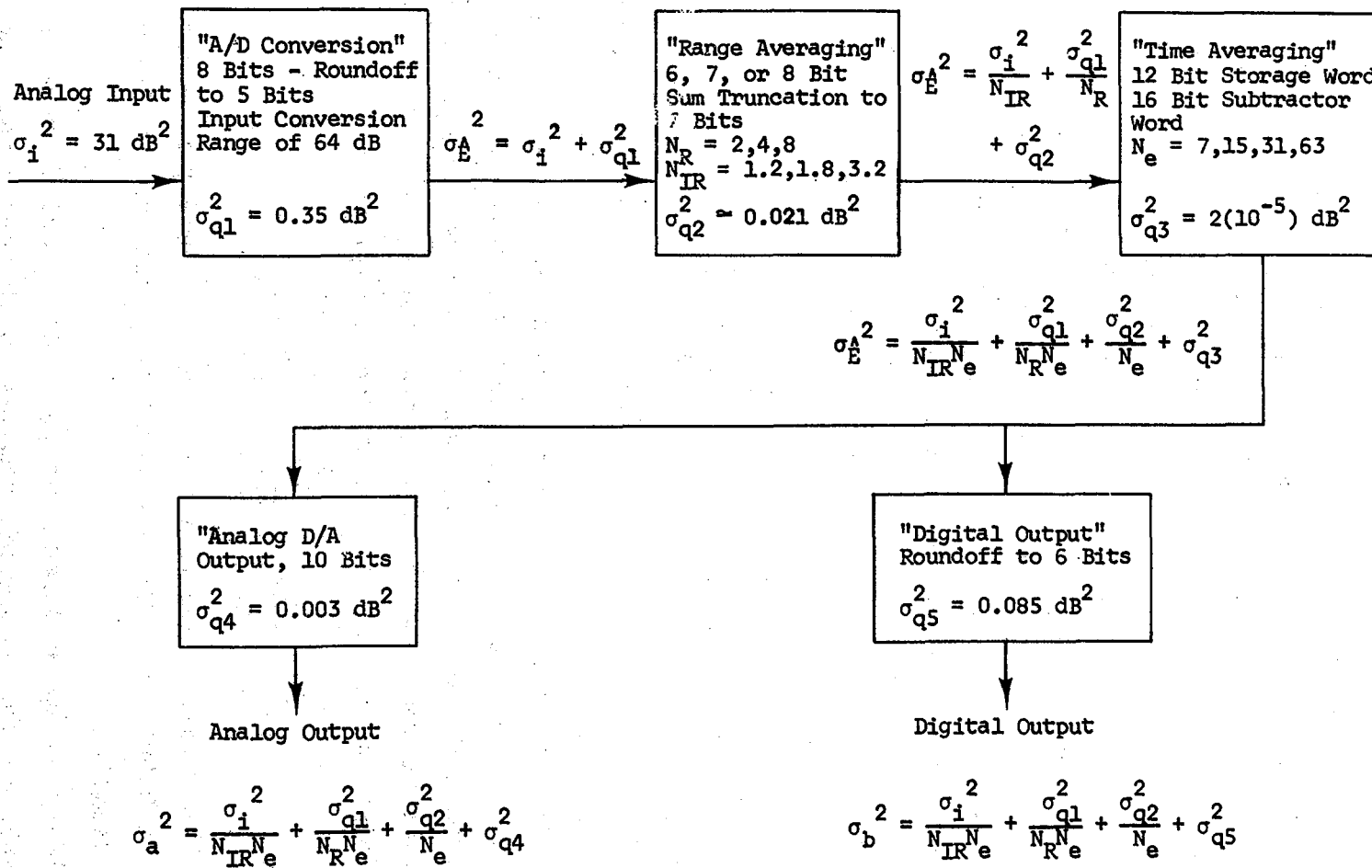


Figure 10. Variance flow diagram for the digital integrator designed for NSSL's WSR-57 radar.

Table 7. Mean Power Estimate Standard Deviation at Analog Output of the WSR-57 Digital Integrator. Table 7 gives S.D. for Various Conditions of Multiplier Constant and Range Averaging Interval.

			Multiplier Constant (B)						
			2^{-2}	2^{-3}	2^{-4}	2^{-5}			
Equivalent Number of Time Samples			7	15	31	63			
Number of Independent Range Samples			STANDARD DEVIATION dB						
Range Interval n. mi.	Number of Independent Range Samples	Equivalent Number of Time Samples	0.25	2	1.2	1.92	1.31	0.91	0.64
0.5	4	1.8	1.57	1.07	0.75	0.52			
1.0	8	3.2	1.18	0.81	0.56	0.39			

Table 8. Mean Power Estimate Standard Deviation of Digital Output of the WSR-57 Digital Integrator. Table 8 gives S.D. for Various Conditions of Multiplier Constant and Range Averaging Interval.

			Multiplier Constant (B)						
			2^{-2}	2^{-3}	2^{-4}	2^{-5}			
Number of Independent Range Samples			7	15	31	63			
Number of Independent Time Samples			STANDARD DEVIATION dB						
Range Interval n. mi.	Number of Independent Range Samples	Number of Independent Time Samples	0.25	2	1.2	1.94	1.34	0.96	0.70
0.5	4	1.8	1.60	1.11	0.80	0.60			
1.0	8	3.2	1.21	0.85	0.63	0.49			

choice of β , the multiplier constant of the time integrator, should be based on the expected Doppler variance (sec. 2.2) from which the statistical behavior of the samples can be predicted and independence or the degree of correlation can be inferred. When the input samples are statistically independent, N_e (derived in sec. 3.2) is the variance reduction. However, pulse-to-pulse correlation decreases the equivalent number of independent time samples. The decrease depends on the degree of correlation and to some extent on the number of samples. Knowing the correlation, we can calculate the number of statistically independent samples from (4) as was done for figure 3. The ratio of the output standard deviation for correlated input samples to the standard deviation assuming statistical independence is shown in figure 11 for an assumed Gaussian input correlation. The standard deviation of the Gaussian correlation is determined by the velocity spectrum standard deviation (Nathanson, 1969). The ratio, shown in figure 11, may be used to adjust the confidence of the mean estimate when the input samples are correlated.

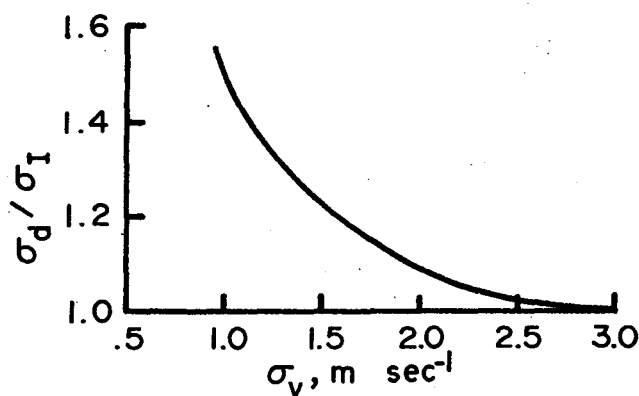


Figure 11. Ratio of the output sample standard deviation for correlated input samples, σ_d , to that obtained for statistically independent samples, σ_I , versus velocity spectrum standard deviation, σ_v . WSR-57 radar parameters assumed.

5.3 Analog Data

5.3.1 Correlation and resolution in azimuth

The two types of output data sets from the integrator are analog (for the display) and digital (for recording). Since these are two different data formats (the analog display is nearly continuous in azimuth and segmented in range; the digital field is segmented in both range and azimuth), the correlation is different for the two data sets. For the analog

display the autocorrelation function in the azimuthal direction is (D.16) in which τ , in terms of angular displacement $\Delta\theta$ and angular velocity Ω , is

$$\tau = \Delta\theta/\Omega .$$

The normalized autocorrelation function of the output between locations spaced $\Delta\theta$ is

$$R_o^{(n)} = \exp \left\{ -\left| \frac{\Delta\theta}{\Omega T_e} \right| \right\} \quad (60)$$

where we assume that the antenna azimuthal beam width is much less than ΩT_e and the input samples are independent. The azimuthal correlation is along arcs of constant range. A quantity of interest is the displacement required for output sample independence. For most practical applications, we consider a data set to be statistically independent if the correlation coefficient between consecutive samples in the series is less than about 0.05 which, from (60), implies an antenna displacement of $\Delta\theta = 3\Omega T_e$. The relationship between the normalized correlation coefficient of the output data and the azimuth displacement between radial samples is shown in figure 12. Since the antenna beam

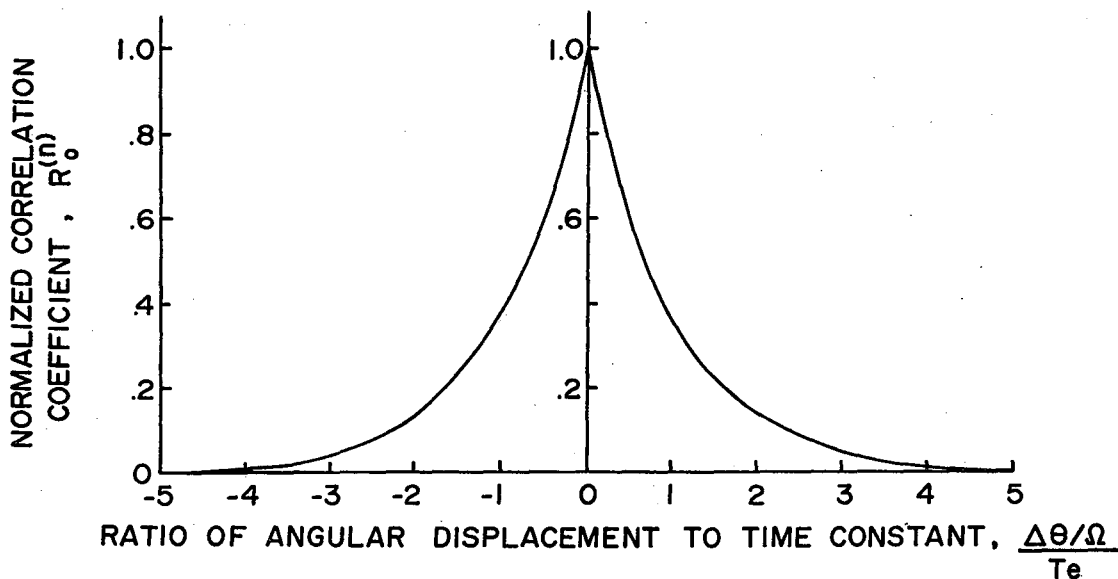


Figure 12. Normalized output autocorrelation coefficient after averaging, $R_o^{(n)}$, versus angular displacement between output samples, $\Delta\theta_o$, for a uniform reflectivity field.

width correlates the output samples as shown in figure 4, the time constant, T_e can be selected so as not to seriously degrade the beam resolution by equating

$$\theta_1 = 3nT_e . \quad (61)$$

The above equation forces equality between the correlation due to beam width and integrator time constant. However, if the T_e is selected on the basis of variance reduction, it is possible that azimuthal resolution would be sacrificed. Otherwise (61) defines a T_e (for given n , θ_1) which in turn fixes power estimate variance. When $\theta_1 \ll 3nT_e$, the spatial resolution of the analog field is dictated by the system transfer function. In terms of the azimuthal angle, this transfer is described by (D.1) where $f = n\theta_s^{-1}$ is substituted (θ_s is the azimuthal scale size). The parameter usually used to describe the "cutoff-scale," θ_{sc} , associated with this type of transfer is the halfpower point.

This occurs at

$$\theta_{sc} = 2\pi n T_e . \quad (62)$$

Thus scale sizes θ_s less than θ_{sc} are effectively filtered (not resolved) because of digital integrator lag. By decreasing T_e , we can increase the resolution of azimuthal scales up to the limit dictated by the beam width.

5.3.2 Correlation and resolution in range

The correlation of analog data sampled in range is, for most practical purposes, equal to unity over the range averaging interval, ΔR , and zero otherwise except for the range interval of 0.25 n miles. Following the methods outlined in appendix C, the correlation between adjacent range averages results in a correlation coefficient of 0.267, 0.067, 0.017, for the 0.25, 0.5, and 1 n mile intervals, respectively. The correlation $\rho(R)$ along the radial coordinate (R) is given, to a good approximation, by

$$\rho(R) = 1 \quad R_c - \frac{\Delta R}{2} \leq R \leq R_c + \frac{\Delta R}{2}$$

$$\rho(R) = 0 \quad \text{otherwise}$$
(63)

when the spatial pulse width is small compared with ΔR . The range, R_c , is to the midpoint of ΔR .

For the above condition, the radial transfer function, $A(K_R)$, is that of a zero order hold (Kuo, 1963), which is given by

$$A(K_R) = \left| \frac{\sin \pi K_R \Delta R}{\pi K_R \Delta R} \right|$$
(64)

where K_R is the radial wave number and, in terms of the range scale size, is $K_R = R_s^{-1}$.

This function is shown in figure 13. The same definition of cut-off applied to (60) produces a cutoff range scale size $R_{sc} = 2.26 \Delta R$. Thus range scale sizes, R_s , smaller than $2.26 \Delta R$ are effectively filtered by the range averaging circuits.

5.4 Digital Data

5.4.1 Correlation and resolution in azimuth

The autocorrelation coefficient and transfer function of the azimuthal coordinate can be derived from (D.16) when the sampling interval is equal to or larger than $3_n T_e$. The numerical value of the correlation coefficient is given by (60) with $\Delta \theta$ equal to the sampling increment.

If the parameter $\Delta \theta / n T_e$ is less than about 3, the resolution

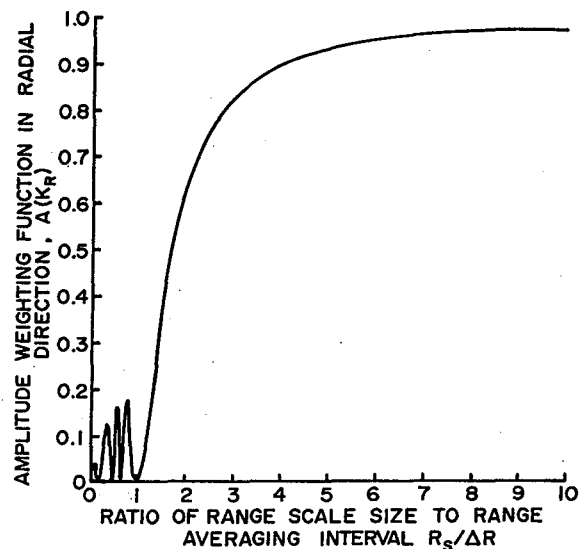


Figure 13. Spatial scale amplitude weighting function along the radial.

of the digital field approaches that of the analog field. If this parameter is greater than about 3, the resolution is determined by the amplitude transfer for a zero order hold at the sampling increment. This transfer function is

$$A(K_\theta) = \left| \frac{\sin \pi K_\theta \Delta\theta}{\pi K_\theta \Delta\theta} \right| \quad (65)$$

where K_θ is the azimuthal wave number and can be expressed in terms of the azimuthal scale size θ_s as

$$K_\theta \equiv \theta_s^{-1}$$

where

$A(K_\theta)$ = amplitude weighting function versus azimuthal wave number

$\Delta\theta$ = sampling increment.

A cutoff scale size, θ_{sc} , is defined in the same manner as the cutoff length for the radial dimension, i.e.,

$$\theta_{sc} = 2.26\Delta\theta \quad (66)$$

The cutoff arclength (S_c) is of course range dependent through the relationship

$$S_c = R\theta_{sc} \quad (67)$$

5.4.2 Correlation and resolution in range

The autocorrelation function and thus the filter function for the radial coordinate is the same as that of the analog data, since the sampling interval is the same. The amplitude weighting function versus radial scale size is shown in figure 13.

5.4.3 Redundancy of the digital data

The amount of redundancy in the digital data may be determined by comparing the variance of the digital field having an autocorrelation coefficient (60) with the variance that would be obtained if the autocorrelation of the data set were zero (statistically independent samples). This expression for the ratio of the number of samples in the set, N_s , to the number of statistically independent samples in the set, N_I , may be obtained by using (4) written here, for convenience, in terms of the output parameters,

$$\frac{\sigma_{oc}^2}{\sigma_o^2} = \frac{N_s}{N_I} = \sum_{k=-(N_s-1)}^{N_s-1} \frac{N_s - |k|}{N_s} R_o^{(n)}(KL) \quad (68)$$

where

σ_{oc}^2 = variance of the output with autocorrelation given by $R_o^{(n)}(KL)$

σ_o^2 = variance of the output with $R_o^{(n)}(KL) = 0$ (independent samples)

N_s = number of output samples in the data set

N_I = number of independent samples in the data set

L = ratio of sampling interval to the effective response time, or in terms of the angular increment; $L = \frac{\Delta\theta}{nT_e}$.

The above ratio is shown in figure 14 as a function of the number of samples in the set and with the autocorrelation coefficient as the variation parameter. The value listed for $R_o^{(n)}$ is the coefficient between adjacent samples ($K = 1$).

The data set may contain from less than 10 to several thousand samples. If the redundancy is to be less than about 30 percent for these sets, then the parameter $L = \Delta\theta/nT_e$ will have to be greater than 2.

6. SAMPLE RESULTS

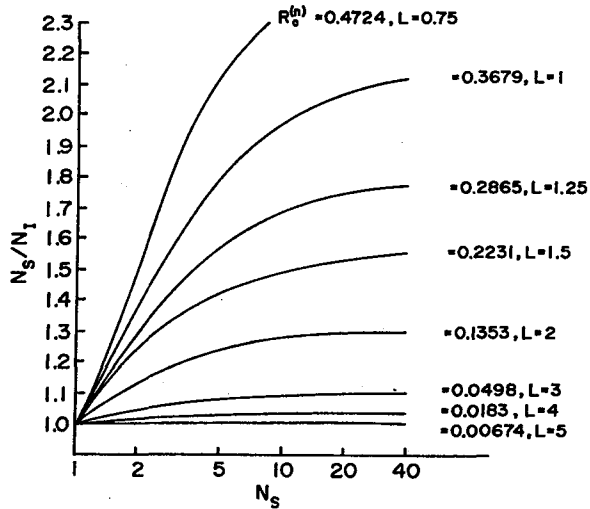


Figure 14. Ratio of number of output samples, N_s , to the number of statistically independent output samples, N_T , as related to the autocorrelation $R_0^{(n)}$ of the azimuthal samples.

A 200 gate digital integrator, with range and time averaging parameters described in the previous section, is interfaced with NSSL's WSR-57 radar. PPI fields of logarithmic power are presented to illustrate reflectivity field characteristics for various range averaging interval and integration time constant combinations. The integrator output is normally categorized in about 10 dB intervals for PPI display so that quantitative estimates of reflectivity and its structure could readily be made.

Nonintegrated, but categorized PPI field of logarithmic echo power estimates are shown in figure 15 which may be compared with integrated echo power fields (fig. 16). Maximum spatial resolution is obtained without integration and thus a nonintegrated power estimate field can form the basis for comparing apparent reflectivity structure. The 4 μ sec pulse width of the WSR-57 radar provides a 600 m range resolution and the radar's antenna provides an angular resolution of 2.2° (3 dB beam width). The $18^\circ/\text{sec}$ rotation rate usually used provides an acquisition time of 123 millisc per sample volume. A photographic film such as figure 15 has effectively integrated the echo samples by continuous film exposure to the light flash of each sample; however, photographic integration does not compromise (for sufficiently small film grain size) spatial resolution which depends only upon radar beam and pulse widths.

Figure 16 shows the echo power field generated when the digital integrator averages power samples in both range and time. Each vertical column of PPI photos corresponds, from left to right, to a

particular range averaging interval of 0.5, 1, and 2 km (1/4, 1/2, and 1 n mile). Averaging time constant changes from 0.022 sec for each display along the top to 0.193 sec along the bottom. Also indicated is the effective number, N_e , of independent samples averaged (sec. 3.2.1) when samples into the time averager are uncorrelated. The sequence of photos were obtained within 4 min. Although the time averaged output is continuously sampled (i.e., digitally integrated output is converted to an analog form) the azimuthal pattern appears "blocky" because echo power categorization causes abrupt light level changes photographed within each range averaging interval.

Time averaged output is also sampled every 2° for magnetic tape storage. At the $18^\circ/\text{sec}$ antenna rotation rate this provides an output sample from each range interval every 0.11 sec, and figure 16 illustrates the reflectivity fields that could be reconstructed from digitally recorded echo power averages.

The range samples are spaced 250 m ($\sim 1/8$ n mile) and because the range averaging interval for 0.5 km (1/4 n mile) is less than the WSR-57 range resolution (600 m), very little compromise in resolution is caused by averaging range samples. As pointed out above, the film integration is active so that the digitally integrated data with $N_e = 7$ or 15 ($\Delta R = 500$ m) should provide resolution similar to that inherent in figure 15. Comparison of figure 16 ($N_e = 7, 15, \Delta R = 500$ m) confirms this deduction. However, as evident in tables 7 and 8, the standard error of power estimate for each sample volume is nearly 2 dB.

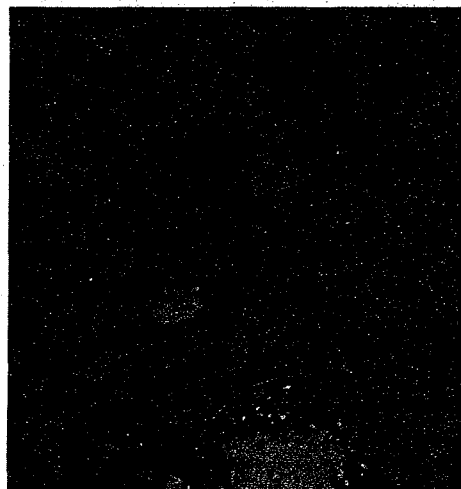
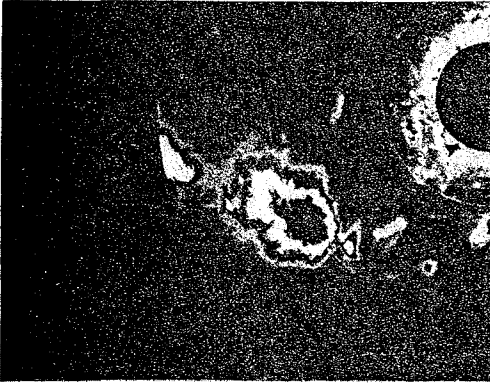


Figure 15. PPI display of nonintegrated logarithmic power resolved by the WSR-57 radar scanning a severe convective storm. Data taken 17:10:55 CST, 4 June 1972. Range marks: 40 km. STC is on; antenna elevation is 0.0° . Brightness level categories are 10 dB wide starting from -85 dBm. Contour code is Dim, Off, Bright,...for increasing power.

$\Delta R = 0.5 \text{ km}$

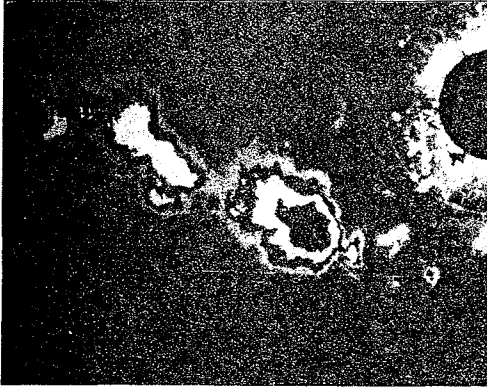


17:09:34

$N_e = 7$

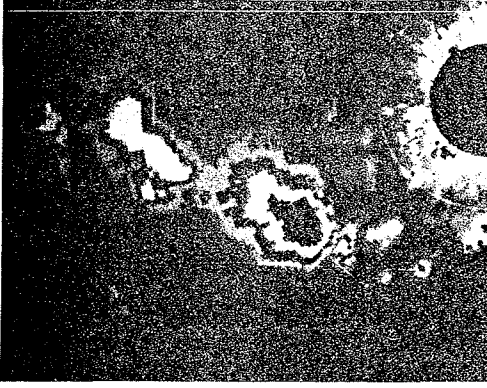
$T_e = 0.022 \text{ sec}$

$\Delta R = 1 \text{ km}$



17:09:54

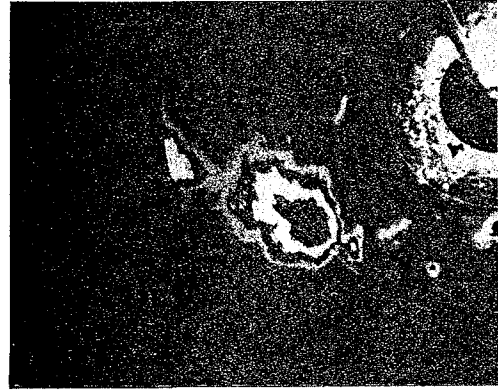
$\Delta R = 2 \text{ km}$



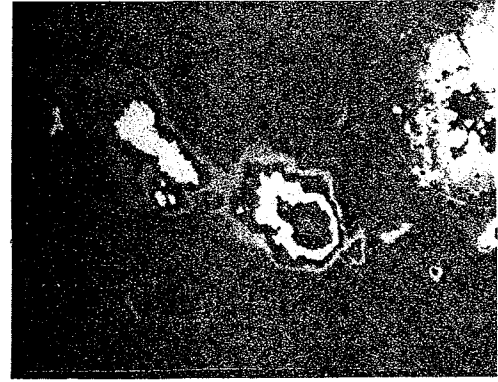
17:10:15

$N_e = 15$

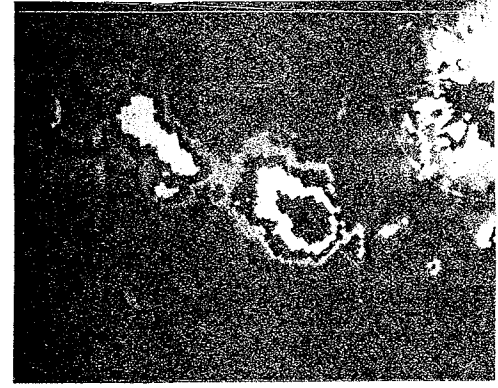
$T_e = 0.046 \text{ sec}$



17:09:14



17:08:54



17:08:34

$N_e = 31$
 $T_e = 0.094 \text{ sec}$



17:07:14



17:06:34



17:06:54

49

$N_e = 63$
 $T_e = 0.193 \text{ sec}$



17:07:34



17:07:54



17:08:14

Figure 16. PPI displays of integrated logarithmic power showing "apparent" reflectivity structure modification with changes in range and time averaging parameters. T_e is the equivalent time constant of digital lowpass filter; N_e is the effective number of independent time samples averaged. Range averaging interval: 0.5, 1, and 2 km. Range marks: 40 km (21.6 n miles). Brightness level categories are: Dim, Light, Off, Bright, ... for boundary power levels of -91, -81, -72, -68, -64 dBm. STC is on. Antenna elevation is 0.0°.

Further reduction in standard error is made with resolution compromise. An increase in time constant to 0.094 sec ($N_e = 31$) and range averaging interval to 1 km ($\sim 1/2$ n mile) produces a spatial resolution degradation of 50 percent (sample volume increases by 50 percent), but standard error of power estimate decreases to 0.8 dB (assuming statistically independent samples into the integrator). The latter time constant and range averaging interval are used in routine data collection at NSSL.

7. CONCLUSIONS AND SUMMARY

This work has shown that digital integrators can be successfully interfaced with the WSR-57 weather radar to reduce the variance of reflectivity estimates without seriously degrading spatial resolution. An exponentially weighted window is used to average samples selected in each of 200 range bins. A multiplier constant (β) of 2^{-4} should provide approximately 31 equivalent independent time samples in the time averager which reduce power estimate variance to less than 1 dB while not compromising the spatial resolution characteristics of the WSR-57 radar. Averages of range samples further help to reduce reflectivity estimate variance for a small loss in range resolution.

Sections 2.1 and 2.2 present a review of the basic statistical properties associated with weather echoes and appendix A relates, in a closed form, the expected value and variance of the mean input power estimate (proportional to reflectivity) for three receiver types (linear, square law, and logarithm). Section 2.3 connects the variance of the input sample mean to the velocity spectrum variance, which in turn is coupled, in sections 2.4 and 2.5, to radar parameters (e.g., beam width, pulse width, etc.) and meteorological status (degree of turbulence, shear, etc.) of the sample volume. The formula $\sigma_v = \sqrt{2 + (4.6 \times 10^{-5}) R_{km}^2}$ m sec⁻¹, derived in section 2.5 and based upon computation and measurement with the WDS-71 Doppler radar provides an estimate of spectrum standard deviation versus range for the WSR-57 radar.

The statistical properties of the echoes and choice of receiver determine the statistical properties of the samples applied to the input of the digital integrator. The large variance (31 dB^2 for a logarithmic receiver) associated with single sample reflectivity estimates dictate that large numbers of input samples need to be averaged. The variance reduction can be achieved by range averaging (sec. 3.1) or by time averaging (sec. 3.2). The merits of range integration and the concomitant loss of range resolution versus the reduction of estimate variance due both to signal variance and receiver noise are presented in sections 3.1.2 and 3.1.3. Estimate bias due to range averaging over regions of reflectivity gradients is derived in appendix B. The characteristics of a digital integrator are derived in section 3.2 and appendix D, where it is shown that the multiplier constant of the digital integrator relates to the integrator time constant (46) and input sample interval (i.e., PRT).

Section 4 derives the variance introduced by the digitization process in the A/D converters, and truncation of words in the time integrator feed-back loop. A variance flow diagram (fig. 10) lists the contribution to estimate variance for the integrator designed for NSSL's WSR-57 radar. The mean power (reflectivity) estimate standard deviation versus multiplier constant and range averaging interval is tabulated in tables 7 and 8.

Characteristics of the output samples and the relation between output correlation and resolution are presented in section 5. It is shown then that variance reduction is achieved at the expense of range and/or azimuthal resolution. A typical output of the integrated analog display is given in section 6 and is compared with unintegrated output.

8. ACKNOWLEDGMENTS

The authors are indebted to many people for their assistance in the preparation of this report, and it would be impossible to acknowledge everyone. However, we would like to thank Mr. Kenneth E. Wilk and Dr. Edwin Kessler for their review and suggestions concerning the report, Mr. Charles Clark and Mrs. Jennifer Farris for the art work, and Mrs. Patricia Nash for her patience in compiling and typing the manuscript.

9. REFERENCES

- Austin, P. M., 1952: A study of the amplitude distribution function for radar echoes from precipitation. Technical Report No. 17, Weather Radar Research, M.I.T., Cambridge, Massachusetts.
- _____, and M. R. Schaffner, 1970: Computation and experiments relevant to digital processing of weather radar echoes. Preprints, Fourteenth Radar Meteorology Conference, Tucson, Arizona, Amer. Meteor. Soc., 375-380.
- Battan, L. J., 1959: Radar Meteorology. University of Chicago Press, Chicago, Illinois.
- Bendat, J. S., and A. G. Piersol, 1971: Random Data: Analysis and Measurement Procedures. Wiley-Interscience, New York, New York.
- Burington, R. S., and D. C. May, 1953: Handbook of Probability and Statistics. Handbook Publishers, Inc., Sandusky, Ohio.
- Crawford, K. C., and R. A. Brown, 1972: Doppler velocity measurements in an approaching squall line. Preprints, Fifteenth Radar Meteorology Conference, Champaign, Illinois, Amer. Meteor. Soc., 27-34.
- Davenport, W. B., and W. L. Root, 1958: Random Signals and Noise. McGraw-Hill Book Company, New York, New York.
- Gold, B., and C. M. Rader, 1969: Digital Processing of Signals. McGraw-Hill Book Company, New York, New York.
- Gradshteyn, I. S., and I. M. Ryzhik, 1965: Table of Integrals, Series, and Products, Fourth Edition. Academic Press, New York, New York.

- Hall, S. F., S. W. Gery, J. P. Bethel, E. M. Drogin, and D. L. Greenberg, 1963: Study of incoherent echo integrator. AFCRL Report No. 3140-1, Air Force Cambridge Research Labs, L. G. Hanscom Field, Bedford, Massachusetts. (Contract AF19(628)-2976)
- Hsu, Hwei P., 1967: Outline of Fourier Analysis. Associated Educational Services Corporation, New York, New York.
- Kerr, D. E., 1951: Propagation of Short Radio Waves. McGraw-Hill Book Company, New York, New York.
- Kuo, B. C., 1963: Analysis and Synthesis of Sampled-Data Control Systems. Prentice-Hall, Inc., Englewood Cliffs, New Jersey.
- Lee, Y. W., 1964: Statistical Theory of Communication. Fourth Edition, John Wiley and Sons, Inc., New York, New York.
- Lhermitte, R. M., 1963: Motions of scatterers and the variance of the mean intensity of weather radar signals. Sperry-Rand Research Center, 5RRC-RR-63-57, Sudbury, Massachusetts.
- _____, and E. Kessler, 1966: Estimation of the average intensity of precipitation targets. Proceedings, Twelfth Radar Meteorology Conference, Norman, Oklahoma, Amer. Meteor. Soc., 23-27.
- Marshall, J. S. and W. Hirschfeld, 1953: Interpretation of the fluctuating echo from randomly distributed scatterers. Part I, Canadian Journal of Physics, 31, 962-995.
- Nathanson, F. E., 1969: Radar Design Principles. McGraw-Hill Book Company, New York, New York.
- Papoulis, A., 1965: Probability, Random Variables, and Stochastic Processes. McGraw-Hill Book Company, New York, New York.
- Rogers, R. R., 1971: The effect of variable target reflectivity on weather radar measurements. Quart. J. Roy. Meteor. Soc., 97, 154-167.
- Silver, S., 1949: Microwave Antenna Theory and Design. McGraw-Hill Book Company, New York, New York.
- Sirmans, Dale, 1968: Note on the distribution of radar return with range. National Severe Storms Laboratory, Norman, Oklahoma, internal memorandum.
- _____, 1970: Special projects at the National Severe Storms Laboratory, the "R" Meter. Report FA-68-WAI-148, Federal Aviation Administration, Systems and Development Service, Washington, D.C., 26 pp.

Smith, P. L., 1964: Interpretation of the fluctuating echo from randomly distributed scatterers: Part 3. McGill University, Stormy Weather Group, Report No. MW-39, Montreal, Canada, 70 pp.

Wallace, P. R., 1953: Interpretation of the fluctuating echo from randomly distributed scatterers, Part II. Canadian Journal of Physics, 31, 995-1009.

Works, G. A., and H. L. Groginsky, 1970: A solid state digital integrator for weather radar signals. Preprints, Fourteenth Radar Meteorology Conference, Tucson, Arizona, Amer. Meteor. Soc., 387-390.

APPENDIX A

COMPARISON OF VARIANCE IN THE POWER ESTIMATES OBTAINED FROM THREE TYPES OF RECEIVERS

In this section we shall derive formula for determining the statistics of input mean power estimates for each of the three receiver types: (1) square law, (2) logarithmic, and (3) linear. Although this problem has been approached by others (Marshall and Hirschfeld, 1953; Smith, 1964) closed-form solutions for the variance of the estimates of the mean have only been obtained for the square law receiver. Smith (1964) conducted a statistical experiment with the aid of a digital computer to determine numerically estimate properties for each of the three receiver types. Thus, no easy and direct comparison of receiver performance is available.

Although a direct numerical solution may be necessary when estimates of the mean input power are formed from k independent sample averages when k is small (i.e., 1, 2, 3...), we shall here provide a closed-form solution, valid for large k , (for practical purpose $k \geq 8$ may be sufficient, Smith, 1964) from which the variances of power estimates can be directly compared.

The large variances of meteorological echo power impose the need to average output voltage samples to obtain satisfactory estimates of the mean input power, \bar{P}_i . The problem is to estimate \bar{P}_i from averages of k independent output samples. The problem of estimation is complicated by the fact that sample averages are performed on the output, W , of a receiver in which W is not linearly related to P_i (except for a square law receiver). Thus an estimate \hat{W}_k

$$\hat{W}_k = \frac{1}{k} \sum_1^k W_k \quad (\text{A.1})$$

of the mean output \bar{W} is made, and then the receiver transfer function is used to obtain an estimate \hat{P}_i , of \bar{P}_i . The problem we address is: Given an output density function having mean \bar{W} and variance σ_w^2 , what is the expected value and variance of the estimate \hat{P}_i obtained from k sample average estimates of \bar{W} ?

A difficult problem is to determine the probability density function of k sample averages of the output when k is a small number. However, by invoking the central limit theorem for large k , this probability density approaches a Gaussian function having a mean equal to the true mean \bar{w} and a variance equal to σ_w^2/k independent of the single sample estimate probability density $f_w(w)$. Thus we shall assume that the output estimates \hat{w}_k have a probability distribution $f(\hat{w}_k)$ given by

$$f(\hat{w}_k) = \exp[-(\hat{w}_k - \bar{w})^2 / 2\sigma_{wk}^2] \quad (\text{A.2a})$$

where

$$\sigma_{wk}^2 = \sigma_w^2 / k. \quad (\text{A.2b})$$

From each estimate \hat{w}_k we obtain, through the receiver transfer characteristic, an estimate \hat{p}_i . The probability density $f(\hat{p}_i)$, not necessarily Gaussian, of the input estimates \hat{p}_i is related to $f(\hat{w}_k)$ as (Papoulis, 1965);

$$f(\hat{p}_i) = \frac{f[\hat{w}_k = g^{-1}(\hat{p}_i)]}{\left| \frac{dg(\hat{w}_k)}{d\hat{w}_k} \right|_{\hat{w}_k = g^{-1}(\hat{p}_i)}} \quad (\text{A.3a})$$

where $\hat{w}_k = g^{-1}(\hat{p}_i)$ is the solution of

$$\hat{p}_i \equiv g(\hat{w}_k) \quad (\text{A.3b})$$

and g^{-1} is the receiver transfer function. In the following, we consider separately the three receiver transfer functions and derive for each the expected value and variance of the estimates \hat{p}_i .

A.1 Square Law Receiver

For the square law receiver, the input power and output voltage relate linearly (see table 2),

$$W = aR_i P_i \quad (\text{A.4})$$

so that the probability density of the input estimate is also Gaussian* with an expected value and standard deviation of \hat{P}_i given by

$$E[\hat{P}_i] = \bar{P}_i \quad (\text{A.5a})$$

$$\sigma = \sqrt{\text{VAR}[\hat{P}_i]} = \frac{\bar{P}_i}{\sqrt{k}} \quad (\text{A.5b})$$

A.2 Logarithmic Receiver

In this case, the receiver input mean power estimate relates to the output mean voltage estimate (see table 2) as

$$\hat{P}_i = \frac{10^{\hat{W}_k/b}}{cR_i} \quad (\text{A.6a})$$

Solving the above for \hat{W}_k

$$\hat{W}_k = b \log cR_i \hat{P}_i \quad (\text{A.6b})$$

and noting that

$$\frac{d\hat{P}_i}{d\hat{W}_k} = \frac{10^{\hat{W}_k/b} \ln 10}{bcR_i} \quad (\text{A.6c})$$

we find that the density function for \hat{P}_i is given by

$$f(\hat{P}_i) = \frac{b/k \exp\{-k[b \log(cR_i \hat{P}_i) - \bar{W}]^2 / 2\sigma_w^2\}}{\sqrt{2\pi} \ln 10 \sigma_w^2 \hat{P}_i} \quad (\text{A.7})$$

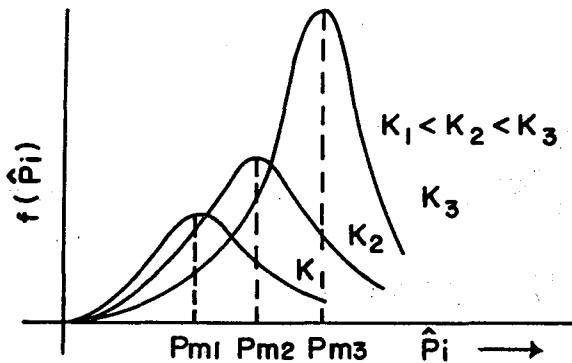
*For the square law receiver, one could just as well use the actual density function of k sample averages from Marshall and Hirschfeld and obtain the results (A.5a) and (A.5b).

The functional form of (A.7) is illustrated graphically in figure A.1. We see from the figure that the most probable estimate P_m of \bar{P}_i asymptotically approaches the value $10^{\bar{W}/b}/cR_i$ as k gets large; that $f(\hat{P}_i)$ is not Gaussian; and \hat{P}_i has a range over all positive values. The expected value and variance estimates \hat{P}_i are found to be

$$E[\hat{P}_i] = \frac{\exp\left\{\frac{\ln 10}{b}\left[\bar{W} + \frac{\sigma_w^2 \ln 10}{2kb}\right]\right\}}{cR_i} \quad (\text{A.8a})$$

$$\text{VAR}[\hat{P}_i] = \frac{\left\{\exp\left[\frac{\sigma_w^2 \ln^2 10}{kb^2}\right] - 1\right\}}{cR_i} \exp\left\{\frac{\ln 10}{b}\left[2\bar{W} + \frac{\ln 10 \sigma_w^2}{kb}\right]\right\} \quad (\text{A.8b})$$

The above expected value and variance of the estimates of \bar{P}_i depend only upon the mean value \bar{W} and variance σ_w^2 of the output random variable W , and these latter parameters are obtained directly from the density function of the single sample estimates in table 2. For Rayleigh input statistics, we have, from table 2,



$$\bar{W} = b \log 0.56 c R_i P_i \quad (\text{A.9a})$$

$$\sigma_w^2 = (0.557)^2 b^2 \quad (\text{A.9b})$$

Substituting (A.9a) into (A.8a) and (A.9b) into (A.8b), respectively, we obtain $E[\hat{P}_i]$ and $\text{VAR}[\hat{P}_i]$ in terms of the true input mean power \bar{P}_i

Figure A.1. Density function, $f(\hat{P}_i)$, for estimates of mean input power.

$$P_m = \left[10^{(\bar{W}/b) - \sigma_w^2 / kb^2 \log e} \right] / cR_i$$

$$E[\hat{P}_i] = 0.56 \bar{P}_i \exp\left\{\frac{0.557 \ln 10}{\sqrt{2k}}\right\}^2 \quad (\text{A.10a})$$

$$\text{VAR}[\hat{P}_i] = E^2[\hat{P}_i] \left[\exp\left\{ \frac{0.557 \ln 10}{\sqrt{k}} \right\}^2 - 1 \right], \quad (\text{A.10b})$$

which in the limit of large k approaches

$$\lim_{k \rightarrow \infty} E[\hat{P}_i] = 0.56 \bar{P}_i \quad (\text{A.11})$$

for the expected value in agreement with the theoretical results of Smith (1964) and experimental results of Lhermitte and Kessler (1966), and

$$\sigma = \sqrt{\text{VAR}[\hat{P}_i]} = 0.72 \bar{P}_i / \sqrt{k} \quad (\text{A.12})$$

for the standard deviation (S.D.) for which there is no closed form results. Note that (A.12) gives the S.D. of the estimates \hat{P}_i about the biased value, $0.56 \bar{P}_i$, of the expected value $E[\hat{P}_i]$. Since the bias is multiplicative, we need to multiply all estimates by a value $(0.56)^{-1}$ to have a more reasonable estimate of \bar{P}_i . It is easy to show that the unbiased estimates \hat{P}'_i , where

$$\hat{P}'_i \equiv \frac{\hat{P}_i}{0.56} \quad (\text{A.13})$$

have a density function similar to (A.7) but have an expected value $E[\hat{P}'_i] = \bar{P}_i$ and a standard deviation

$$\text{VAR}^{\frac{1}{2}}[\hat{P}'_i] = \frac{0.72 \bar{P}_i}{0.56 \sqrt{k}} = \frac{1.28 \bar{P}_i}{\sqrt{k}}. \quad (\text{A.14})$$

Since the square law receiver provides an unbiased estimate of \bar{P}_i , it is convenient to compare (A.14), the S.D. of the unbiased estimate obtained with a logarithmic receiver, with (A.7b), the unbiased estimate with a square law receiver.

A.3 Linear Receiver

For the case of a linear receiver, the output W linearly relates to input voltage amplitude V_i . Again by invoking the central limit theorem, we assume that the density function of the output estimates, from k sample averages, can be expressed by the Gaussian density (A.2a) where

$$\hat{W}_k = \frac{1}{k} \sum_1^k W_k \equiv a \hat{V}_i \quad (\text{A.15})$$

is an estimate of \bar{W} ; σ_w is the S.D. of the samples W (before averaging); and \bar{W} is the mean value of the output samples W . Assuming Rayleigh distributed input statistics (see table 2);

$$\bar{W} = \frac{a\sqrt{\pi R_i \bar{P}_i}}{2} \quad (\text{A.16a})$$

$$\sigma_w = \frac{a}{2} \sqrt{(4-\pi) R_i \bar{P}_i} \quad (\text{A.16b})$$

where \bar{P}_i is the input mean power. From each of the output estimates, we find (through the receiver transfer characteristics) an estimate \hat{P}_i of \bar{P}_i . That is

$$\hat{P}_i = \frac{\hat{W}_k^2}{R_i} = \frac{\hat{W}_k^2}{a^2 R_i} \equiv g(\hat{W}_k) .$$

Applying (A.3) we get the following density function for the \hat{P}_i 's

$$f(\hat{P}_i) = k^{\frac{1}{2}} [2\pi(4-\pi)\bar{P}_i \hat{P}_i]^{-\frac{1}{2}} \exp\left\{-\frac{2k}{(4-\pi)\bar{P}_i} \left[\hat{P}_i^{\frac{1}{2}} - \sqrt{\frac{\pi}{4}} \bar{P}_i^{\frac{1}{2}}\right]^2\right\} . \quad (\text{A.17})$$

The expected value of \hat{P}_i is found by applying (A.17) to the equation

$$E[\hat{P}_i] = \int_0^{\infty} \hat{P}_i f(\hat{P}_i) d\hat{P}_i ,$$

which upon integration (Gradshteyn and Ryzhik, 1965, 3.642(1)) yields

$$E[\hat{P}_i] = \frac{\sqrt{2k} \bar{P}_i \{\exp(-\frac{Z}{4})\} D_{-3}(-Z^{\frac{1}{2}})}{4Z} \quad (\text{A.18})$$

where $Z = k\pi(4-\pi)$ and $D_{-3}(-Z^{\frac{1}{2}})$ is a parabolic cylinder function. For large k , we use the asymptotic expansions of D (Gradshteyn and Ryzhik, 1965, 9.246(2)) and retain only the principal terms to arrive at

$$\lim_{k \rightarrow \infty} E[\hat{P}_i] = \frac{\pi}{4} \bar{P}_i, \quad (\text{A.19})$$

which shows that the \hat{P}_i 's are biased estimators. Equation (A.19) agrees with the experimental result of Austin (1952).

The variance of the estimates \hat{P}_i is found by applying the formula

$$\text{VAR}[\hat{P}_i] = E[\hat{P}_i^2] - E^2[\hat{P}_i] \equiv \sigma^2. \quad (\text{A.20})$$

Upon evaluation, we find that σ^2 is given approximately by

$$\sigma^2 \approx \frac{0.67 \bar{P}_i^2}{k}.$$

Since we have a biased estimator, the S.D. of the unbiased estimates is given by

$$\text{VAR}^{\frac{1}{2}}[\hat{P}'_i] = \frac{1.05 \bar{P}_i}{\sqrt{k}}. \quad (\text{A.21})$$

The statistical properties of \hat{P}'_i (in particular the variance) have not been numerically investigated by Smith. However, Marshall and Hitschfeld's calculations indicate that amplitude averages might lead to a better estimate of \bar{P}_i than averages of the logarithmic receiver output. Comparisons of (A.21) with (A.14) reinforce the use of amplitude averages. It is understood from the comparison that the average of linear receiver output samples produces a S.D. in the estimates of \bar{P}_i quite close to that of the ideal square law receiver. For the logarithmic

receiver to produce the same S.D. as a linear receiver, we need to process

$$\frac{\text{VAR}[P'_i]_{\text{log}}}{\text{VAR}[P'_i]_{\text{lin}}} = \left(\frac{1.28}{1.05}\right)^2 = 1.5$$

or 50 percent more independent samples.

APPENDIX B

BIAS IN RANGE AVERAGES DUE TO REFLECTIVITY GRADIENTS

In this appendix, we discuss the mean power estimate bias caused by range averaging the logarithmic receiver output. Two range dependent reflectivity models are assumed in order to obtain limits on the averaging volume range size for given spatial variations of the reflectivity field.

We define range averaging bias ϵ_R as the dB difference between two quantities: (1) the logarithm of the spatial average of mean power ($\log \bar{P}$), and (2) the spatial average of the logarithm of mean power ($\overline{\log P}$). That is,

$$\epsilon_R = 10 \left[\log_{10} \left\{ \frac{1}{\Delta R} \int_{R_0}^{R_0 + \Delta R} \bar{P}_i(R) dR \right\} - \frac{1}{\Delta R} \int_{R_0}^{R_0 + \Delta R} \log_{10} \bar{P}_i(R) dR \right] \text{ dB} . \quad (\text{B.1})$$

The first term on the right of (B.1) is the true average (in dB) while the second term is that calculated from logarithmic receiver output averages. The digital integrator averages single sample estimates of $\log P_i$ (the range averaged estimates of $\log P_i$ are then averaged in time), but it is easily shown that the order of time and range average is immaterial. Therefore, for sake of simplicity, we assume the reflectivity field to be time averaged before range averaging (i.e., bar over \bar{P}_i indicates time average).

A first and simple model to visualize is a step increase in reflectivity or echo power. This is the same as Rogers Model 1 (Rogers, 1971). Although not physically realizable, this could be a reasonable approximation of the reflectivity field if the extent of the gradient were small compared with the range averaging interval and may be appropriate at the boundaries of severe storm cells.

To derive the bias, assume a return power range dependence as shown in figure B.1. The spatial average of echo power is

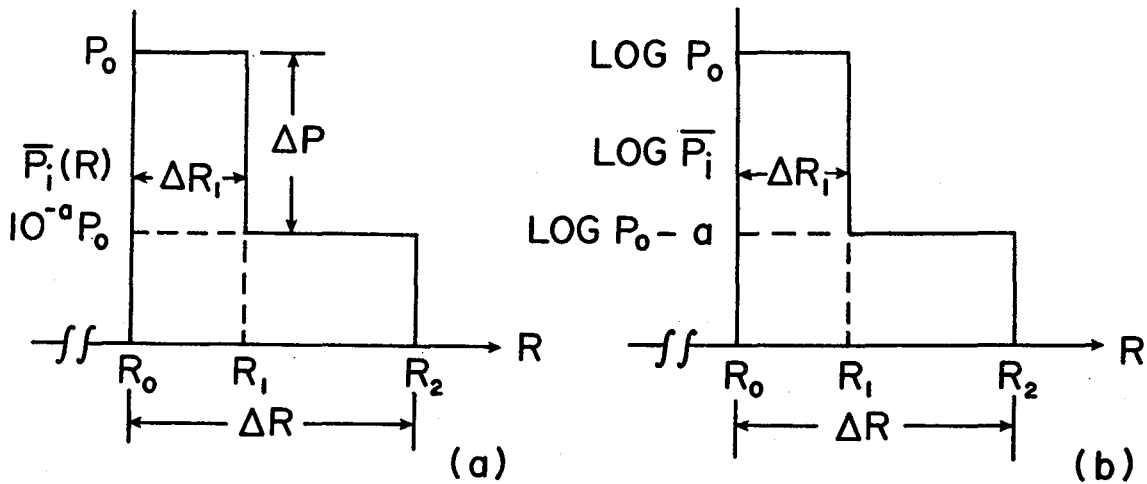


Figure B.1. Range dependency of mean (time averaged) echo power (a), and logarithm of echo power (b) for a step change in reflectivity.

$$\langle \bar{P}_i(R) \rangle \equiv \frac{1}{R_2 - R_0} \int_{R_0}^{R_2} \bar{P}_i(R) dR = P_0 \left\{ \frac{\Delta R_1}{\Delta R} (1 - 10^{-a}) + 10^{-a} \right\} \quad (B.2)$$

where the brackets denote range averaging. The spatial average of the logarithm of return power is

$$\langle \log \bar{P}_i(R) \rangle \equiv \frac{1}{R_2 - R_0} \int_{R_0}^{R_2} \log \bar{P}_i(R) dR = \log P_0 - a \left(1 - \frac{\Delta R_1}{\Delta R} \right) \quad (B.3)$$

Therefore the dB bias ϵ_R is

$$\epsilon_R = 10 \left[\log \left[\frac{\Delta R_1}{\Delta R} (1 - 10^{-a}) + 10^{-a} \right] + a \left(1 - \frac{\Delta R_1}{\Delta R} \right) \right] \quad (B.4)$$

Equation (B.4) is plotted in figure B.2 as a function of $\Delta R_1/\Delta R$ for various values of the parameter "10a" in terms of dB of mean return power step. Figure B.2 shows that the bias is maximum when the range interval is less than half filled with power P_0 . This is because the

logarithm function gives nonuniform weight to the power distribution, resulting in disproportionately larger weight for smaller powers. For similar reasons the bias is always positive (dB), which indicates the spatial average of the logarithm of return power always underestimates the true spatial average power.

A more physically satisfying model of reflectivity field has no discontinuities in reflectivity or its gradients. An exponential spatial distribution of reflectivity meets these requirements, and biases in estimates of average reflectivity will now be determined for this case (Rogers Model 3). The spatial distribution of mean return power with range is depicted in figure B.3(a) and is expressed functionally as

$$\bar{P}_i(R) = P_0 10^{b(R-R_0)} \quad (B.5)$$

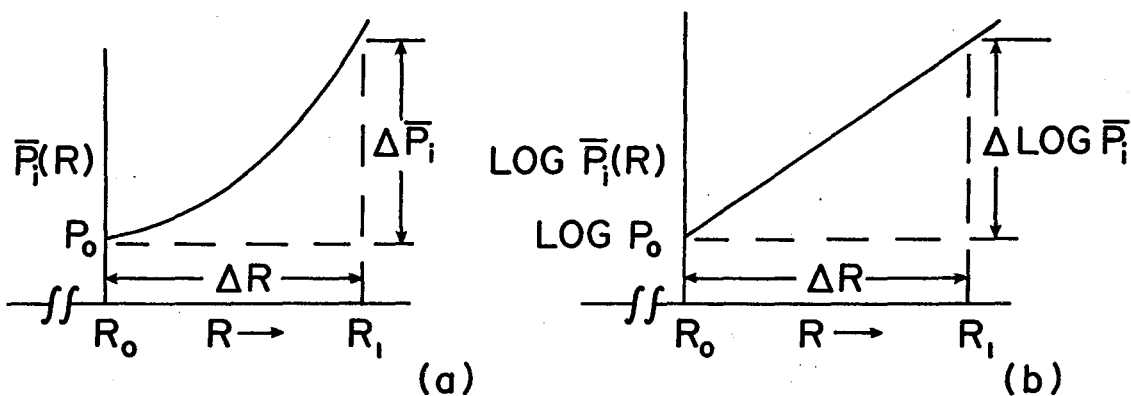


Figure B.3. Range dependency of echo power (a), and logarithm of echo power (b) for an assumed exponential reflectivity distribution.

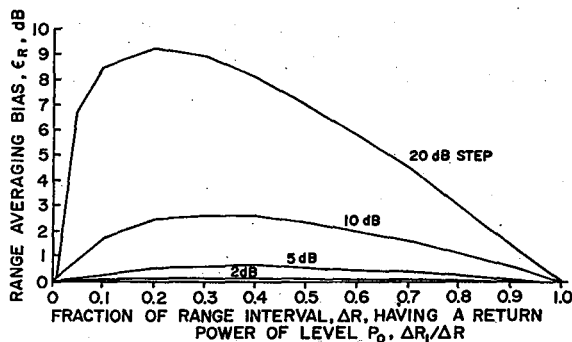


Figure B.2. Range averaging bias for a step change in reflectivity versus range interval ΔR_i having echo power 10^a times the balance of the averaging interval ΔR .

where b = range power gradient and is assumed constant over the averaging interval $\Delta R = R_1 - R_0$. The spatial distribution of the logarithm \bar{P}_i is depicted in figure B.3(b) and is expressed functionally as

$$\log \bar{P}_i(R) = \log P_0 + b(R - R_0) \quad (B.6)$$

where $b = \frac{10}{dR} \frac{d(\log \bar{P})}{\text{km}} \frac{\text{dB}}{\text{km}}$ is the constant gradient of \log (reflectivity) and b is the power change, expressed in dB, across ΔR . Of course, (B.6) applies for negative gradients.

The spatial average of $\bar{P}_i(R)$ is given by

$$\langle \bar{P}_i(R) \rangle = \frac{10 P_0 (10^{b\Delta R/10} - 1)}{b\Delta R \ln 10} \quad (B.7)$$

whereas the spatial average of $\log \bar{P}_i(R)$ is

$$\langle \log \bar{P}_i(R) \rangle = \log P_0 + \frac{b\Delta R}{20} \quad (B.8)$$

Using (B.1) the bias is

$$\epsilon_R = 10 \left[1 - \frac{b\Delta R}{20} + \log \left(\frac{10^{b\Delta R/10} - 1}{b\Delta R \ln 10} \right) \right] \text{ dB} \quad (B.9)$$

It can easily be shown that (B.9) is symmetric with respect to b , and hence (B.9) can be used as well for negative gradient values. It is interesting to note that the bias magnitude depends on the total change of mean power within ΔR , which is given by power gradient-range increment product. Assuming that the actual reflectivity distribution can be well approximated by segments of exponential functions, the bias in each segment would be related by (B.9) to the power difference across each segment. Hence estimation of errors in averaging the total reflectivity field may be determined. Equation (B.9) is plotted in figure B.4, and since the bias is always positive, the estimates of the mean power returned from an averaging volume will be biased below the true mean value.

The expected gradient for an entire data field will be a constraint on the maximum range averaging interval. Measurements at NSSL on five storms with a range interval of 8 μ sec yielded an expected bias of 0.75 dB to 1.25 dB due to this effect (Sirmans, 1968). Measurements made at the Applied Physics Laboratory (Nathanson, 1969) indicate a predicated bias of less than 0.5 dB over an 8 μ sec range interval.

The bias of a particular range increment could be very large compared with the average error for the reflectivity field. Sirmans noted biases as large as 12 dB, and Rogers (1971) reports range power gradients that would result in even larger values.

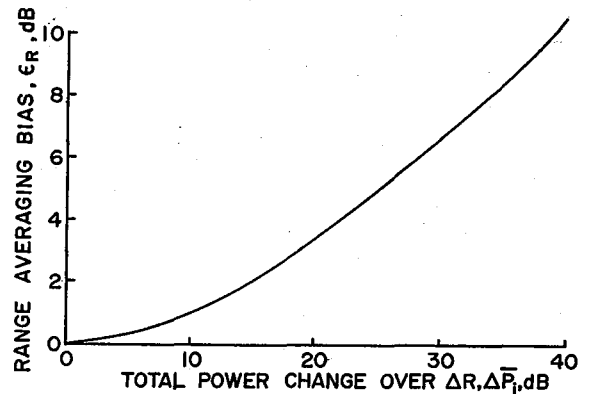


Figure B.4. Range averaging bias for an exponential range power distribution.

APPENDIX C

AUTOCORRELATION OF RANGE SAMPLES

Assuming a reflectivity field with "white noise" properties (i.e., power scattered from contiguous differential volumes are uncorrelated) and a rectangular transmitter pulse, the normalized autocorrelation function of the echo samples are derived herein. An echo sample is the ensemble sum of signals returned from each differential volume having a range extent dR and an angular extent determined by the antenna beam width. The ensemble average extends over the number of dR 's contained in the interval $c\tau_p/2$. We shall derive the correlation between these ensemble averages using the methods outlined by Burington and May (1953).

We assume the signal associated with each differential volume to be statistically independent and the ensemble to contain k contiguous complex samples from the series,

$$x_1, x_2, x_3, \dots, x_u, x_{u+1}, \dots, x_k, x_{k+1}, \dots, x_{k+u-1}$$

where x_k is the signal associated with the k^{th} differential volume. The k sample ensemble is

$$S_k(u) = \frac{1}{k} \sum_{j=u}^{k+u-1} x_j \quad u = 1, 2, 3, \dots \quad (\text{C.1})$$

where u is a number proportional to the sample increment range location. The correlation between averages $S(1)$ and $S(u)$ where

$$S_k(1) = \frac{1}{k} \sum_{i=1}^k x_i \quad S_k(u) = \frac{1}{k} \sum_{j=u}^{k+u-1} x_j \quad (\text{C.2})$$

can be expressed as (Burington and May, 1953, p. 131)

$$\rho(k,u) = \frac{\text{Cov } [x_i, x_j]}{[\text{Var } x_i \text{ Var } x_j]^{\frac{1}{2}}} \quad (\text{C.3})$$

If the mean and variance of the two averages are the same (i.e., uniform reflectivity field), the denominator of (C.3) reduces to

$$\text{Var } [x_i] = \text{Var } [x_j] = \sigma^2 . \quad (\text{C.4})$$

The numerator is the covariance of the two series that can be expressed in terms of the correlation, ρ_{ij} , between samples comprising the series and the sample standard deviation as

$$\text{Cov } [x_i, x_j] = \rho_{ij} \sigma_i \sigma_j . \quad (\text{C.5})$$

Because we have assumed statistical independence between differential volumes and equality of the standard deviation, then,

$$\begin{aligned} \sigma_i &= \sigma_j = \sigma \\ \rho_{ij} &= 1 && i = j \\ \rho_{ij} &= 0 && i \neq j . \end{aligned} \quad (\text{C.6})$$

Noting that $i = j$ for the number of "common" samples $k-u+1$, (C.3) reduces to

$$\rho(k,u) = \frac{(k-u+1) \sigma^2}{\sigma^2} = k-u+1 . \quad (\text{C.7})$$

The normalized correlation is given by

$$\frac{\rho(k,u)}{\rho(k,1)} = \frac{k-u+1}{k} . \quad (\text{C.8})$$

The length of the k sample ensemble average is proportional to the sample volume depth, $c\tau_p/2$, and $u-1$ is proportional to the spacing $c\tau_s/2$ between range samples. This results in a signal autocorrelation, $\rho_s(\tau_s)$, which varies with τ_s as

$$\rho_s(\tau_s) = \frac{k-u+1}{k} = 1 - \frac{|\tau_s|}{\tau_p} \quad 0 < |\tau_s| < \tau_p \cdot$$

$$= 0 \quad \text{otherwise} \quad (C.9)$$

If the mean reflectivity varies with range, the means of the ensemble averages will not be the same and the variances will increase over the variance for uniform reflectivity by an amount depending on the mean reflectivity variation. The autocorrelation (C.9), derived for the receiver input signal amplitude is, for sake of simplicity, assumed to be the correlation of samples at the receiver output. Although the assumption is valid for a linear receiver, a rigorous treatment needs to treat the correlation transformation through a logarithmic receiver (Davenport and Root, 1958).

APPENDIX D

PROPERTIES OF THE DIGITAL LOWPASS FILTER

The lowpass RC filter is extensively analyzed in the engineering literature, and the digital integration in time (pulse to pulse) may be described more readily by the equivalent continuous analog approximation than by the rigorous Z-transform theory required for the sampled case (Gold and Rader, 1969). The problem is to find a digital loop that has a system function (the Fourier Transform of the unit impulse response) equal to the sampled system function of the lowpass RC filter. First consider the system frequency response $H_a(f)$ of the lowpass RC filter given by (Hsu, 1967),

$$H_a(f) = \frac{1}{1 + j2\pi f T_e} \quad (D.1)$$

where T_e is the time constant of the RC filter.

Consider now the recursive digital lowpass filter described by the algorithm (Bendat and Piersol, 1971, eq. 9.31)

$$y_n = \beta x_n + (1 - \beta) y_{n-1} \quad (D.2)$$

where

$$y_n = n^{\text{th}} \text{ output}$$

$$x_n = n^{\text{th}} \text{ input}$$

and where β is a positive constant less than one, which we will write for convenience in the form

$$\beta = 1 - \exp\left[-\frac{T_s}{T_e}\right]. \quad (D.3)$$

The frequency response, $H_D(f)$, of the digital filter is given by (Bendat and Piersol, 1971, eq. 9.32)

$$H_D(f) = \frac{\beta}{1 - (1-\beta) \exp[-j2\pi f T_s]} \quad (D.4)$$

which under the restrictions, $T_e \gg T_s$ and $2\pi f T_s \ll 1$, (D.4) may be expressed as

$$H_D(f) \approx \frac{1}{1 + j2\pi f T_e} \quad (D.5)$$

Thus the digital lowpass transfer function approximates the analog under the above restrictions. The equivalent time constant, T_e , of the digital lowpass filter is obtained in terms of the digital multiplier constant, β , and the sampling interval, T_s , by solving (D.3)

$$T_e = \frac{T_s}{\ln(1 - \beta)^{-1}} \quad (D.6)$$

Expanding $\ln(1 - \beta)^{-1}$ in a Taylor series, we get

$$\ln(1 - \beta)^{-1} = -\ln(1 - \beta) = \beta + \frac{\beta^2}{2} + \frac{\beta^3}{3} + \dots$$

Hence,

$$T_e = \frac{T_s}{\sum_{n=1}^{\infty} \frac{\beta^n}{n}} \quad (D.7)$$

The ratio of T_e to T_s for the values of β used in the WSR-57 processor is given in table D.1. Note that truncating the series to the first two terms approximates the quantity T_e/T_s by $N_e/2$ (i.e., (45)), and that this approximation is within 0.6 percent of the exact value for the worst case ($\beta = 2^{-2}$).

We will now derive two parameters of an equivalent analog RC filter that will be helpful in specifying the statistical properties of the digital integrator. These are: (1) equivalent integration

Table D.1. Equivalent Time Constant for the WSR-57 Processor.

Multiplier Constant (β)	Number of Samples in Time Average (N_e)	$\frac{T_e}{T_s}$	$\frac{N_e}{2}$
2^{-2}	7	3.48	3.5
2^{-3}	15	7.49	7.5
2^{-4}	31	15.49	15.5
2^{-5}	63	31.5	31.5

time and (2) autocorrelation of the output. Both will be calculated for a statistically independent (white noise) input signal.

The equivalent integration time, T_a , i.e., the width of the equivalent rectangular time window, can be derived by equating the mean square output voltage, $y^2(t)$, to the mean square input voltage, $x^2(t)$, averaged with uniform weighting for a time T_a .

$$\overline{y^2(t)} = \frac{1}{T_a} \int_{-T_a/2}^{T_a/2} \overline{x^2(t)} dt . \quad (D.8)$$

Equation (D.8) expresses the conservation of energy where $\overline{y^2} = \overline{x^2}$ for the assumed stationary random process. The mean square input voltage is given by the autocorrelation of white noise at zero lag (Hsu, 1967, eq. 7.129)

$$\overline{x^2(t)} = K \delta(0) \quad (D.9)$$

where K is the constant spectral density and $\delta(t)$ is the delta function. The mean square output voltage is given by (Hsu, 1967, eq. 7.149)

$$\overline{y^2(t)} = \frac{K}{2T_e} . \quad (D.10)$$

Substituting (D.10) and (D.9) into (D.8) and solving for T_a , we have

$$\frac{K}{2T_e} = \frac{1}{T_a} \int_{-T_a/2}^{T_a/2} K \delta(0) dt = \frac{K}{T_a}$$

or

$$T_a = 2T_e . \quad (D.11)$$

Thus the equivalent integration time is twice the time constant of the lowpass RC filter, or, in other words, T_a is the width of an equivalent rectangular time window needed to achieve the same variance reduction of output as a lowpass analog filter with time constant T_e .

The autocorrelation function, $R_o(\tau)$, of the filter output is (Hsu, 1967)

$$R_o(\tau) = \int_{-\infty}^{\infty} h(t) \int_{-\infty}^{\infty} h(\sigma) R_i(\tau + \sigma - t) d\sigma dt \quad (D.12)$$

where $h(t)$ is the unit impulse response of the filter (i.e., $h(t) = 1/T_e \exp[-t/T_e]$, $t \geq 0$), R_i is the autocorrelation of the input signal,

$$R_i(\tau) = K \delta(\tau) , \quad (D.13)$$

$\delta(\tau)$ is the Dirac delta function, and K is a constant equal to the spectral density. Thus for a lowpass RC filter the autocorrelation of the output is given by

$$R_o(\tau) = \int_0^{\infty} \frac{1}{T_e} \exp\left[-\frac{\tau}{T_e}\right] \int_0^{\infty} \frac{K}{T_e} \exp\left[-\frac{\sigma}{T_e}\right] \delta(\tau + \sigma - t) d\sigma dt ,$$

which after a certain amount of perseverance can be shown to be

$$\frac{K}{2T_e} [1 - \exp(-2t_1/T_e)] \exp(-\tau/T_e) \quad (D.14)$$

where t_1 is the time after the first sample entered the integrator (i.e., time at which first output sample is taken) and $\tau = t_2 - t_1$ ($t_2 > t_1$) is the interval between samples. For steady state (i.e., $t_1 \rightarrow \infty$),

$$R_o(\tau) = \frac{K}{2T_e} \exp[-\frac{\tau}{T_e}] . \quad (D.15)$$

For practical purposes the steady state is assumed to be achieved (i.e., 95 percent of $R_o(\tau)$) at a time $3T_e$ from the first sample entered the integrator. The normalized autocorrelation function is given by

$$R_o^{(n)}(\tau) = \frac{R_o(\tau)}{R_o(0)} = \exp[-\frac{\tau}{T_e}] . \quad (D.16)$$

The value of the normalized autocorrelation function at the output sampling interval is the correlation coefficient of the output data set sampled at intervals τ_s .

Although the above is derived for an assumed analog filter, the results apply to the digital integrator if T_e is taken from (46) as the digital integrator time constant and used in (D.16).

APPENDIX E

CUMULATIVE DISTRIBUTION FOR THE PROBABILITY DENSITY OF THE LOGARITHM OF ECHO POWER

The following tabulation is the cumulative distribution of $\log P_i$ used to calculate the relative frequency of occurrences of the digital classes necessary to determine the digital integrator output-mean power input estimate transfer integrator characteristic. The boundary values, t_m, t_{m+1} , of the m^{th} digital class are defined in dB units above (or below) the mean input power. The value t_m for any input mean power (\bar{P}_i) is given by the difference $B_m - 10 \log \bar{P}_i$. The area tabulated (table E.1) is the integral value of $\text{Prob}[\log P_i / \bar{P}_i]$ between $-\infty$ and t_m , where $-\infty$ is the lower bound of the zeroth class. The relative frequency of occurrence (F_m) of the m^{th} class for a given \bar{P}_i is

$$F_m = \int_{-\infty}^{t_{m+1}} \text{Prob}[\log P] d \log P - \int_{-\infty}^{t_m} \text{Prob}[\log P] d \log P .$$

This is shown graphically in figure E.1. The digital output average, \bar{X} , corresponding to a given mean power input is

$$\bar{X} = \sum_{m=0}^M F_m \cdot m$$

where

\bar{X} = digital output for a given mean power input

m = digital class weight

M = number of digital classes

B_m = digital class boundary in dBm.

Table E.1. Cumulative Distribution of Probability Density of the
 Logarithm of Echo Power. Area = $\int_{-\infty}^{t/10} \text{Prob}(x) dx$ *

t	Area	t	Area	t	Area	t	Area
-25.0	.0030	-16.0	.0247	-7.0	.1808	2.0	.7947
-24.5	.0034	-15.5	.0276	-6.5	.2005	2.5	.8307
-24.0	.0038	-15.0	.0310	-6.0	.2220	3.0	.8637
-23.5	.0043	-14.5	.0347	-5.5	.2455	3.5	.8930
-23.0	.0048	-14.0	.0389	-5.0	.2710	4.0	.9185
-22.5	.0055	-13.5	.0435	-4.5	.2986	4.5	.9399
-22.0	.0061	-13.0	.0487	-4.0	.3284	5.0	.9573
-21.5	.0069	-12.5	.0545	-3.5	.3602	5.5	.9708
-21.0	.0078	-12.0	.0610	-3.0	.3941	6.0	.9810
-20.5	.0087	-11.5	.0682	-2.5	.4301	6.5	.9882
-20.0	.0098	-11.0	.0762	-2.0	.4678	7.0	.9931
-19.5	.0110	-10.5	.0851	-1.5	.5073	7.5	.9961
-19.0	.0124	-10.0	.0950	-1.0	.5480	8.0	.9980
-18.5	.0139	-9.5	.1060	-0.5	.5897	8.5	.9990
-18.0	.0156	-9.0	.1182	0.0	.6320	9.0	.9995
-17.5	.0175	-8.5	.1316	0.5	.6742	9.5	.9997
-17.0	.0196	-8.0	.1465	1.0	.7158	10.0	.9998
-16.5	.0220	-7.5	.1628	1.5	.7562		

*Prob(x) = $m \exp [m(x-x_0) - \exp m(x-x_0)]$, and $x = \log P_i$,
 $x_0 = \log \bar{P}_i$, $m = \ln 10$, $t = 10 x$.

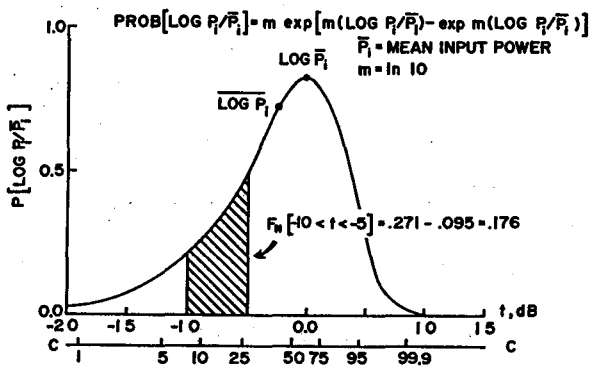


Figure E.1. Probability distribution of $\log P_i/\bar{P}_i$. Shaded area is the probability that $-10 < 10 \log (P_i/\bar{P}_i) < -5$. Scale C is the probability, in percent, that $10 \log P_i/\bar{P}_i$ is less than the value on the t axis.

NATIONAL SEVERE STORMS LABORATORY

The NSSL Technical Memoranda, beginning with No. 28, continue the sequence established by the U. S. Weather Bureau National Severe Storms Project, Kansas City, Missouri. Numbers 1-22 were designated NSSP Reports. Numbers 23-27 were NSSL Reports, and 24-27 appeared as subseries of Weather Bureau Technical Notes. These reports are available from the National Technical Information Service, Operations Division, Springfield, Virginia 22151, for \$3.00, and a microfiche version for \$0.95. NTIS numbers are given below in parentheses.

- No. 1 National Severe Storms Project Objectives and Basic Design. Staff, NSSP. March 1961. (PB-168207)
- No. 2 The Development of Aircraft Investigations of Squall Lines from 1956-1960. B. B. Goddard. (PB-168208)
- No. 3 Instability Lines and Their Environments as Shown by Aircraft Soundings and Quasi-Horizontal Traverses. D. T. Williams. February 1962. (PB-168209)
- No. 4 On the Mechanics of the Tornado. J. R. Fulks. February 1962. (PB-168210)
- No. 5 A Summary of Field Operations and Data Collection by the National Severe Storms Project in Spring 1961. J. T. Lee. March 1962. (PB-165095)
- No. 6 Index to the NSSP Surface Network. T. Fujita. April 1962. (PB-168212)
- No. 7 The Vertical Structure of Three Dry Lines as Revealed by Aircraft Traverses. E. L. McGuire. April 1962. (PB-168213)
- No. 8 Radar Observations of a Tornado Thunderstorm in Vertical Section. Ralph J. Donaldson, Jr. April 1962. (PB-174859)
- No. 9 Dynamics of Severe Convective Storms. Chester W. Newton. July 1962. (PB-163319)
- No. 10 Some Measured Characteristics of Severe Storms Turbulence. Roy Steiner and Richard H. Rhyne. July 1962. (N62-16401)
- No. 11 A Study of the Kinematic Properties of Certain Small-Scale Systems. D. T. Williams. October 1962. (PB-168216)
- No. 12 Analysis of the Severe Weather Factor in Automatic Control of Air Route Traffic. W. Boynton Beckwith. December 1962. (PB-168217)
- No. 13 500-Kc./Sec. Sferics Studies in Severe Storms. Douglas A. Kohl and John E. Miller. April 1963. (PB-168218)
- No. 14 Field Operations of the National Severe Storms Project in Spring 1962. L. D. Sanders. May 1963. (PB-168219)
- No. 15 Penetrations of Thunderstorms by an Aircraft Flying at Supersonic Speeds. G. P. Roys. Radar Photographs and Gust Loads in Three Storms of 1961 Rough Rider. Paul W. J. Schumacher. May 1963. (PB-168220)
- No. 16 Analysis of Selected Aircraft Data from NSSP Operations, 1962. T. Fujita. May 1963. (PB-168221)
- No. 17 Analysis of Methods for Small-Scale Surface Network Data. D. T. Williams. August 1963. (PB-168222)
- No. 18 The Thunderstorm Wake of May 4, 1961. D. T. Williams. August 1963. (PB-168223)
- No. 19 Measurements by Aircraft of Condensed Water in Great Plains Thunderstorms. George P. Roys and Edwin Kessler. July 1966. (PB-173048)
- No. 20 Field Operations of the National Severe Storms Project in Spring 1963. J. T. Lee, L. D. Sanders and D. T. Williams. January 1964. (PB-168224)
- No. 21 On the Motion and Predictability of Convective Systems as Related to the Upper Winds in a Case of Small Turning of Wind with Height. James C. Fankhauser. January 1964. (PB-168225)
- No. 22 Movement and Development Patterns of Convective Storms and Forecasting the Probability of Storm Passage at a Given Location. Chester W. Newton and James C. Fankhauser. January 1964. (PB-168226)
- No. 23 Purposes and Programs of the National Severe Storms Laboratory, Norman, Oklahoma. Edwin Kessler. December 1964. (PB-166675)
- No. 24 Papers on Weather Radar, Atmospheric Turbulence, Sferics, and Data Processing. August 1965. (AD-621586)
- No. 25 A Comparison of Kinematically Computed Precipitation with Observed Convective Rainfall. James C. Fankhauser. September 1965. (PB-168445).

- No. 26 Probing Air Motion by Doppler Analysis of Radar Clear Air Returns. Roger M. Lhermitte. May 1966. (PB-170636)
- No. 27 Statistical Properties of Radar Echo Patterns and the Radar Echo Process. Larry Armijo. May 1966. The Role of the Kutta-Joukowski Force in Cloud Systems with Circulation. J. L. Goldman. May 1966. (PB-170756)
- No. 28 Movement and Predictability of Radar Echoes. James Warren Wilson. November 1966. (PB-173972)
- No. 29 Notes on Thunderstorm Motions, Heights, and Circulations. T. W. Harrold, W. T. Roach, and Kenneth E. Wilk. November 1966. (AD-644899)
- No. 30 Turbulence in Clear Air Near Thunderstorms. Anne Burns, Terence W. Harrold, Jack Burnham, and Clifford S. Spavins. December 1966. (PB-173992)
- No. 31 Study of a Left-Moving Thunderstorm of 23 April 1964. George R. Hammond. April 1967. (PB-174681)
- No. 32 Thunderstorm Circulations and Turbulence from Aircraft and Radar Data. James C. Fankhauser and J. T. Lee. April 1967. (PB-174860)
- No. 33 On the Continuity of Water Substance. Edwin Kessler. April 1967. (PB-175840)
- No. 34 Note on the Probing Balloon Motion by Doppler Radar. Roger M. Lhermitte. July 1967. (PB-175930)
- No. 35 A Theory for the Determination of Wind and Precipitation Velocities with Doppler Radars. Larry Armijo. August 1967. (PB-176376)
- No. 36 A Preliminary Evaluation of the F-100 Rough Rider Turbulence Measurement System. U. O. Lappe. October 1967. (PB-177037)
- No. 37 Preliminary Quantitative Analysis of Airborne Weather Radar. Lester P. Merritt. December 1967. (PB-177188)
- No. 38 On the Source of Thunderstorm Rotation. Stanley L. Barnes. March 1968. (PB-178990)
- No. 39 Thunderstorm - Environment Interactions Revealed by Chaff Trajectories in the Mid-Troposphere. James C. Fankhauser. June 1968. (PB-179659)
- No. 40 Objective Detection and Correction of Errors in Radiosonde Data. Rex L. Inman. June 1968. (PB-180284)
- No. 41 Structure and Movement of the Severe Thunderstorms of 3 April 1964 as Revealed from Radar and Surface Mesonetwork Data Analysis. Jess Charba and Yoshikazu Sasaki. October 1968. (PB-183310)
- No. 42 A Rainfall Rate Sensor. Brian E. Morgan. November 1968. (PB-183979)
- No. 43 Detection and Presentation of Severe Thunderstorms by Airborne and Ground-Based Radars: A Comparative Study. Kenneth E. Wilk, John K. Carter, and J. T. Dooley. February 1969. (PB-183572)
- No. 44 A Study of a Severe Local Storm of 16 April 1967. George Thomas Haglund. May 1969. (PB-184-970)
- No. 45 On the Relationship Between Horizontal Moisture Convergence and Convective Cloud Formation. Horace R. Hudson. March 1970. (PB-191720)
- No. 46 Severe Thunderstorm Radar Echo Motion and Related Weather Events Hazardous to Aviation Operations. Peter A. Barclay and Kenneth E. Wilk. June 1970. (PB-192498)
- No. 47 Evaluation of Roughness Lengths at the NSSL-WKY Meteorological Tower. Leslie D. Sanders and Allen H. Weber. August 1970. (PB-194587)
- No. 48 Behavior of Winds in the Lowest 1500 ft in Central Oklahoma: June 1966 - May 1967. Kenneth C. Crawford and Horace R. Hudson. August 1970.
- No. 49 Tornado Incidence Maps. Arnold Court. August 1970. (COM-71-00019)
- No. 50 The Meteorologically Instrumented WKY-TV Tower Facility. John K. Carter. September 1970. (COM-71-00108)
- No. 51 Papers on Operational Objective Analysis Schemes at the National Severe Storms Forecast Center. Rex L. Inman. November 1970. (COM-71-00136)
- No. 52 The Exploration of Certain Features of Tornado Dynamics Using a Laboratory Model. Neil B. Ward. November 1970. (COM-71-00139)
- No. 53 Rawinsonde Observation and Processing Techniques at the National Severe Storms Laboratory. Stanley L. Barnes, James H. Henderson and Robert J. Ketchum. April 1971.

- No. 54 Model of Precipitation and Vertical Air Currents. Edwin Kessler and William C. Bumgarner. June 1971.
- No. 55 The NSSL Surface Network and Observations of Hazardous Wind Gusts. Operations Staff. June 1971.
- No. 56 Pilot Chaff Project at the National Severe Storms Laboratory. Edward A. Jessup. November 1971.
- No. 57 Numerical Simulation of Convective Vortices. Robert P. Davies-Jones and Glenn T. Vickers. November 1971.
- No. 58 The Thermal Structure of the Lowest Half Kilometer in Central Oklahoma: December 9, 1966 - May 31, 1967. R. Craig Goff and Horace R. Hudson. July 1972.
- No. 59 Cloud-to-Ground Lightning Versus Radar Reflectivity in Oklahoma Thunderstorms. Gilbert D. Kinzer. September 1972.
- No. 60 Simulated Real Time Displays of Velocity Fields by Doppler Radar. L. D. Hennington and G. B. Walker. November 1972.
- No. 61 Gravity Current Model Applied to Analysis of Squall-Line Gust Front. Jess Charba. November 1972.
- No. 62 Mesoscale Objective Map Analysis Using Weighted Time-Series Observations. Stanley L. Barnes. March 1973.
- No. 63 Observations of Severe Storms on 26 and 28 April 1971. Charles L. Vicek. April 1973.